

Základy petrologie sedimentárních hornin

1.roč., LS

3) Karbonáty I.- komponenty,
struktury, sedimentační prostředí

Karel Martínek

ÚGP

(Ústav geologie a paleontologie)

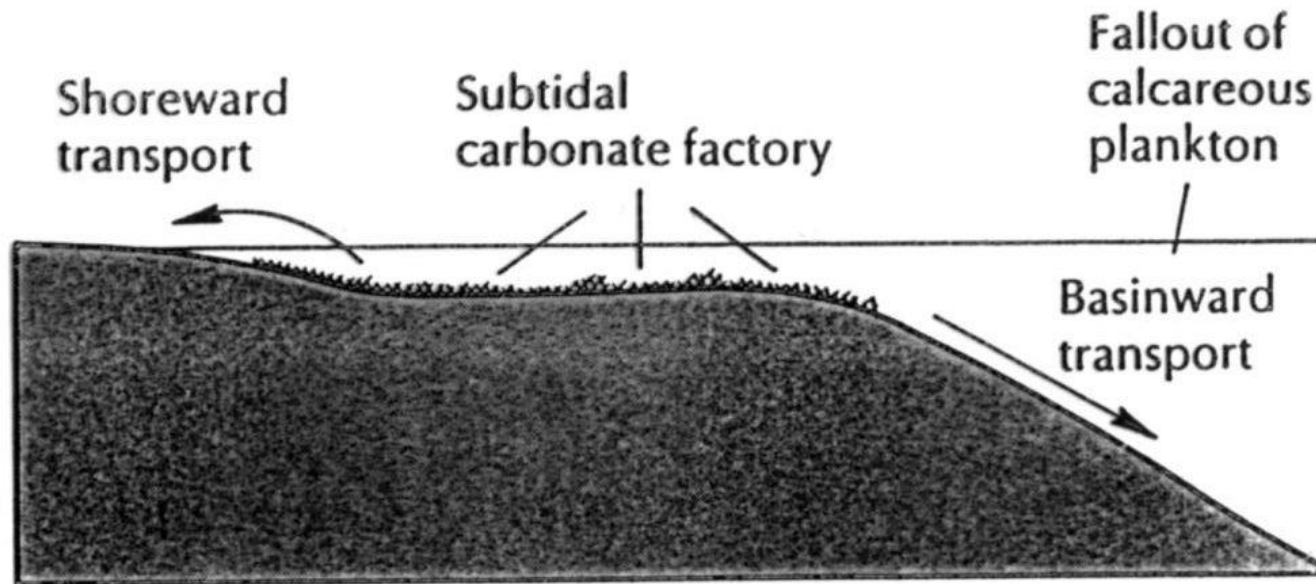


Figure 6.1

Sketch of carbonate shelf, showing main regions of accumulation of carbonate sediments. From James (1984).

mineralogie

kalzit (low Mg, high Mg), aragonit, dolomit

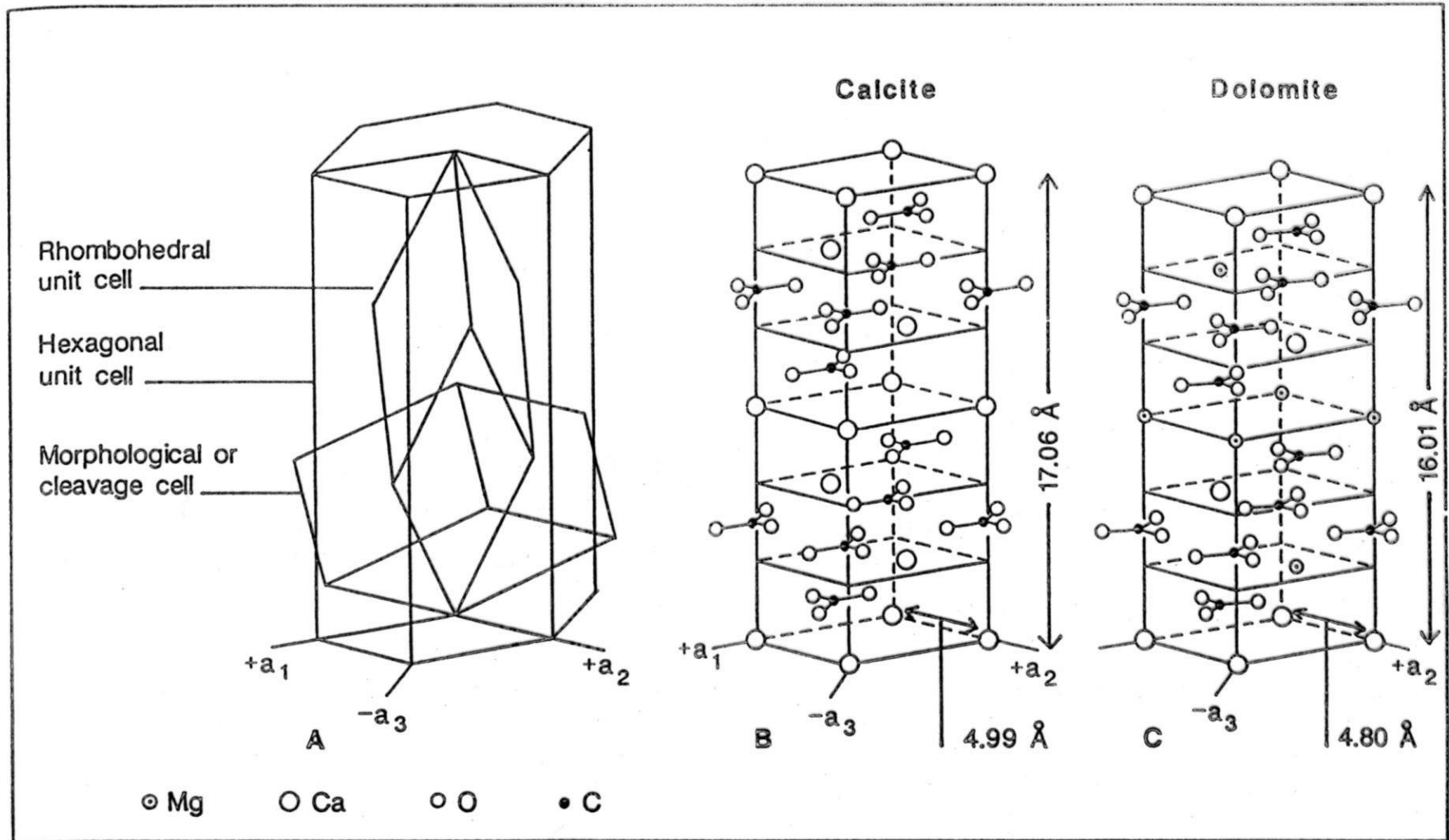


Fig. 6.1 (A) Diagrammatic relationship between rhombohedral, hexagonal and morphological unit cells and the hexagonal crystallographic axes. (B) Hexagonal unit cell of calcite, apparent rectilinear shape due to perspective; a_1 , a_2 and $a_3 = 4.99 \text{ \AA}$; $c = 17.06 \text{ \AA}$. (C) Hexagonal unit cell of dolomite; a_1 , a_2 and $a_3 = 4.80 \text{ \AA}$; $c = 16.01 \text{ \AA}$.

komponenty

zrna (klasty): ooidy, pisoidy, peloidy, agregáty, intraklasty, bioklasty, řasy; stromatolity;
mezizrnová hmota: matrix (karbonátový kal) nebo tmel (cement, spartit); Folkova
klasifikace (1962)

ooidy

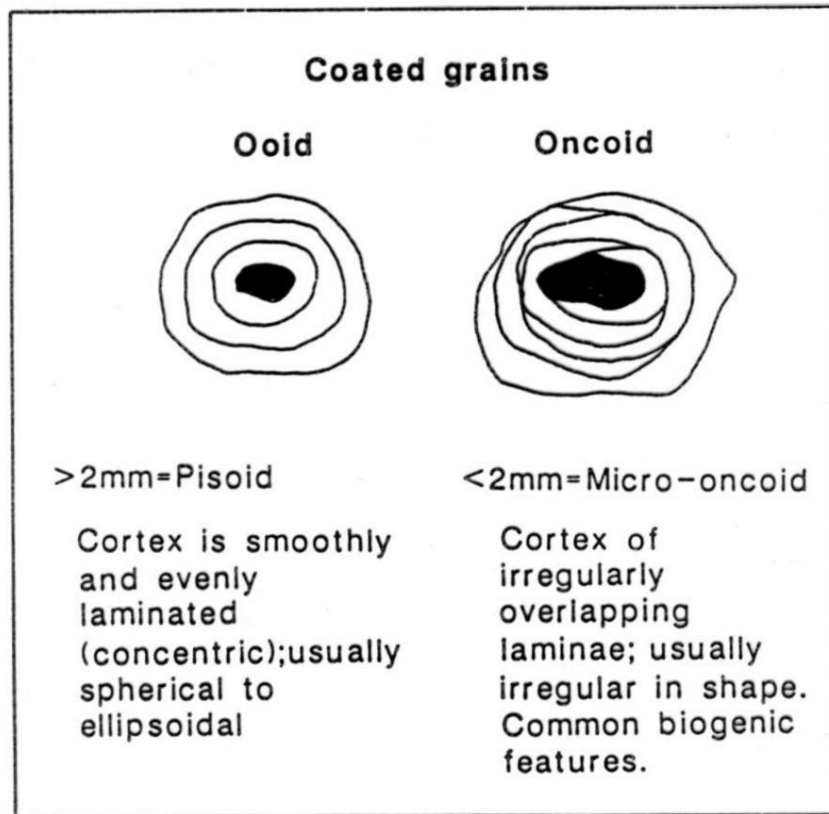


Fig. 1.1 Classification of coated grains.

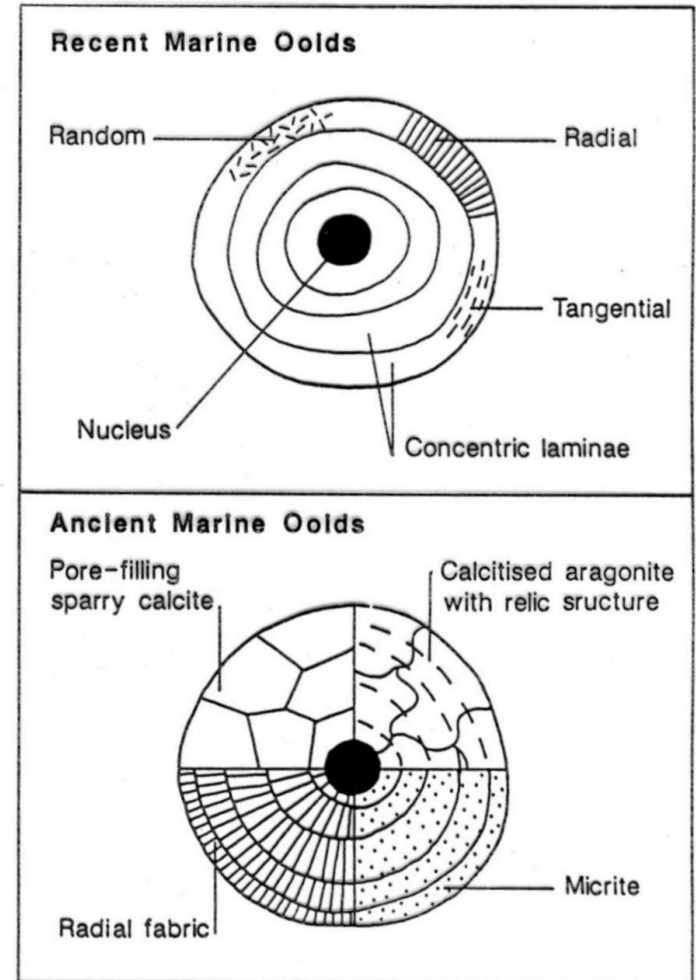


Fig. 1.2 Major types of microstructure seen in modern and ancient ooids. Variations on these types have been described from ancient ooids by Tucker (1984), Strasser (1986), Chow & James (1987) and Singh (1987).

peloidy

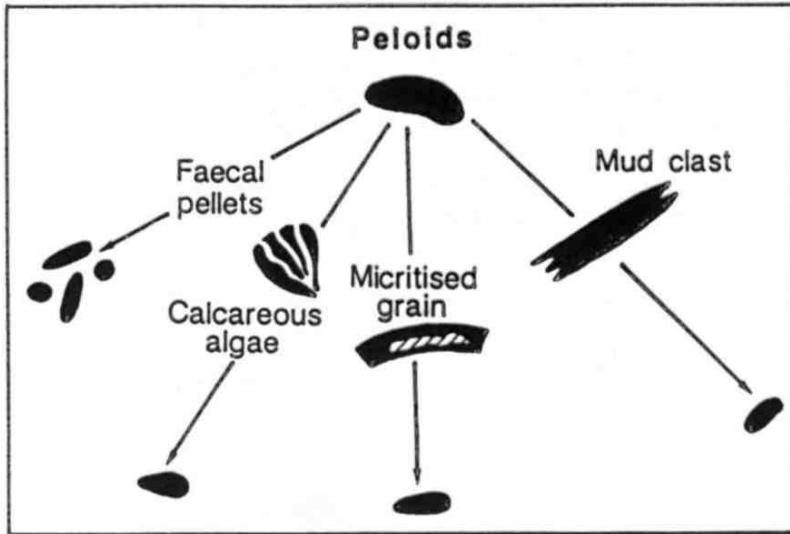


Fig. 1.7 *Origins of peloids.*

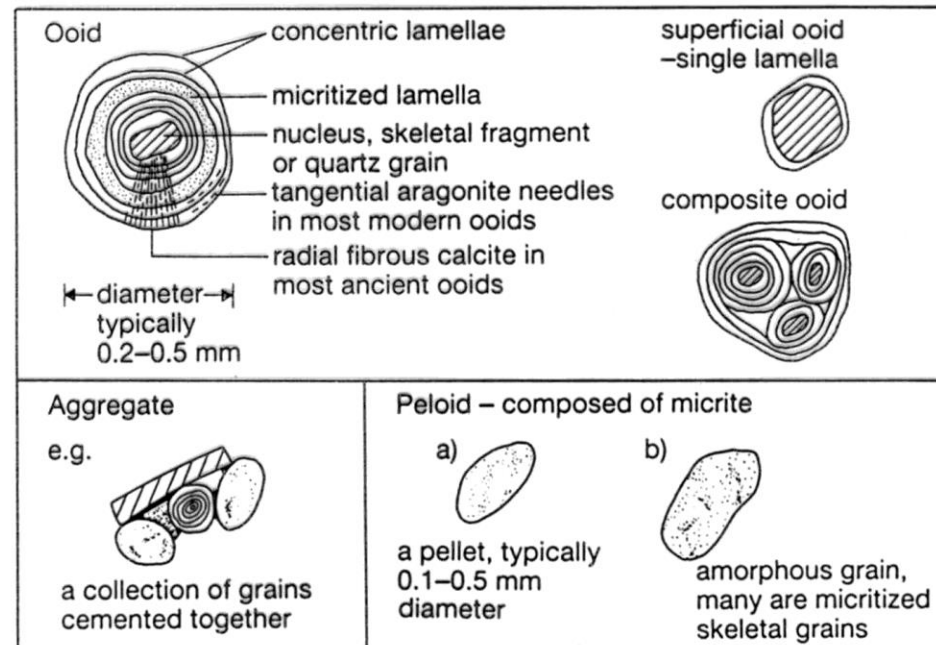


Fig. 4.1 The principal non-skeletal grains in limestones: ooids, peloids and aggregates.

Table 4.1 The mineralogy of carbonate skeletons (x = dominant mineralogy, (x) = less common). During diagenesis, these mineralogies may be altered or replaced; in particular, aragonite is metastable and is invariably replaced by calcite, and high-Mg calcite loses its Mg

bioklasty

Organism	Mineralogy			
	Aragonite	Low-Mg calcite	High-Mg calcite	Aragonite + calcite
Mollusca:				
bivalves	x	x		x
gastropods	x			x
pteropods	x			
cephalopods	x		(x)	
Brachiopods		x	(x)	
Corals:				
scleractinian	x			
rugose + tabulate		x	x	
Sponges	x	x	x	
Bryozoans	x		x	x
Echinoderms			x	
Ostracods		x	x	
Foraminifera:				
benthic	(x)		x	
pelagic		x		
Algae:				
coccolithophoridae		x		
rhodophyta	x		x	
chlorophyta	x			
charophyta		x		

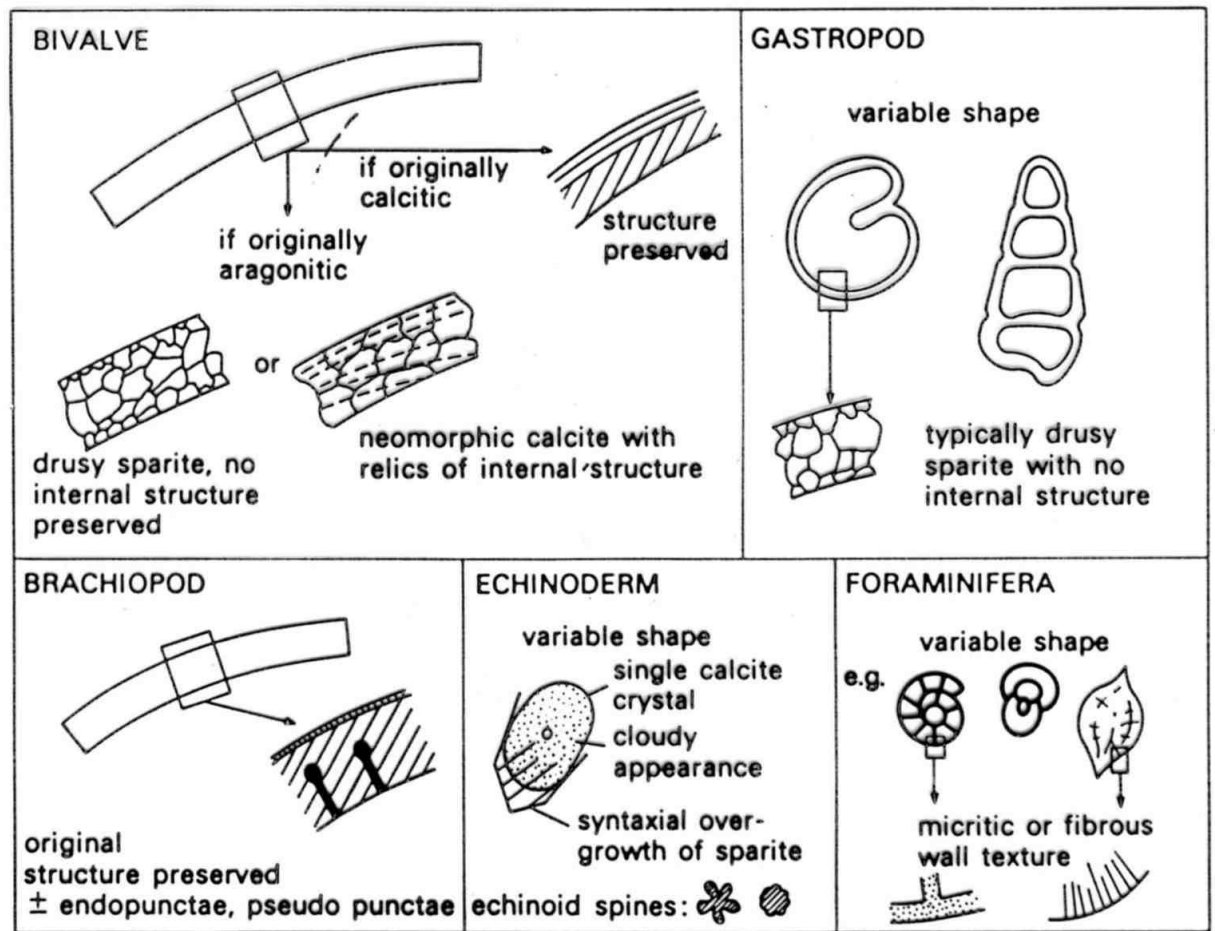


Fig. 4.9 Typical thin-section appearance of bivalve, gastropod, brachiopod, echinoderm and foraminiferal skeletal grains in limestone.

Molluscan aragonite shell replacement

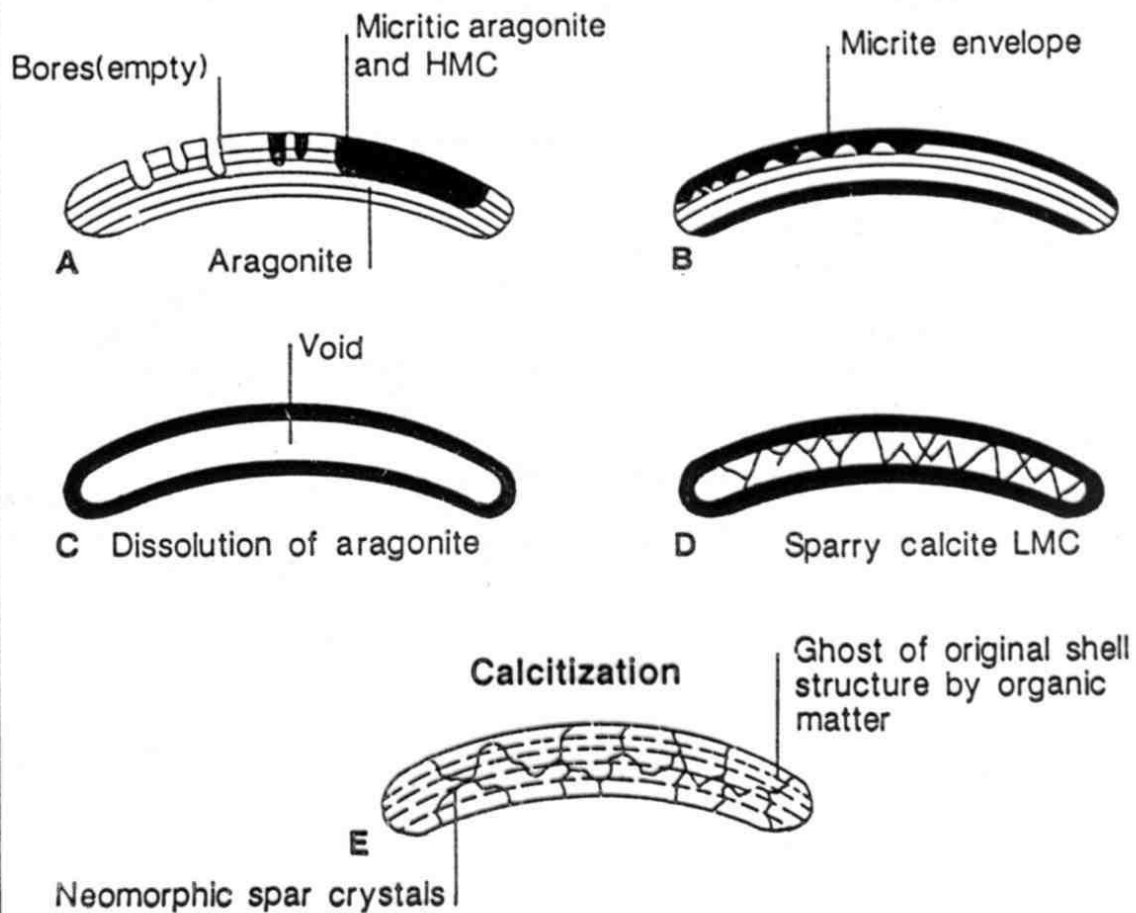


Fig. 1.10 Molluscan aragonite shell replacement. (A–D) By a dissolution–cementation process. (E) By calcitization with the preservation of relic microarchitecture (see text and Section 7.2).

horninotvorné organismy (vápňité schránky)

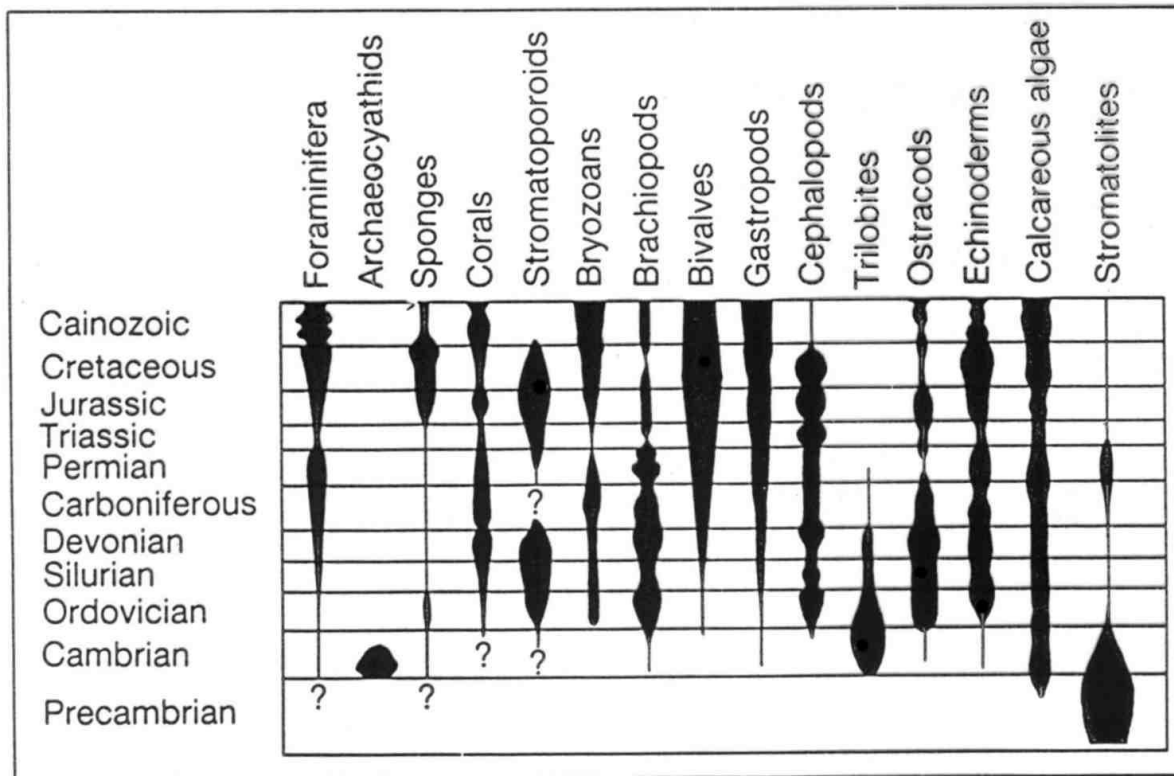
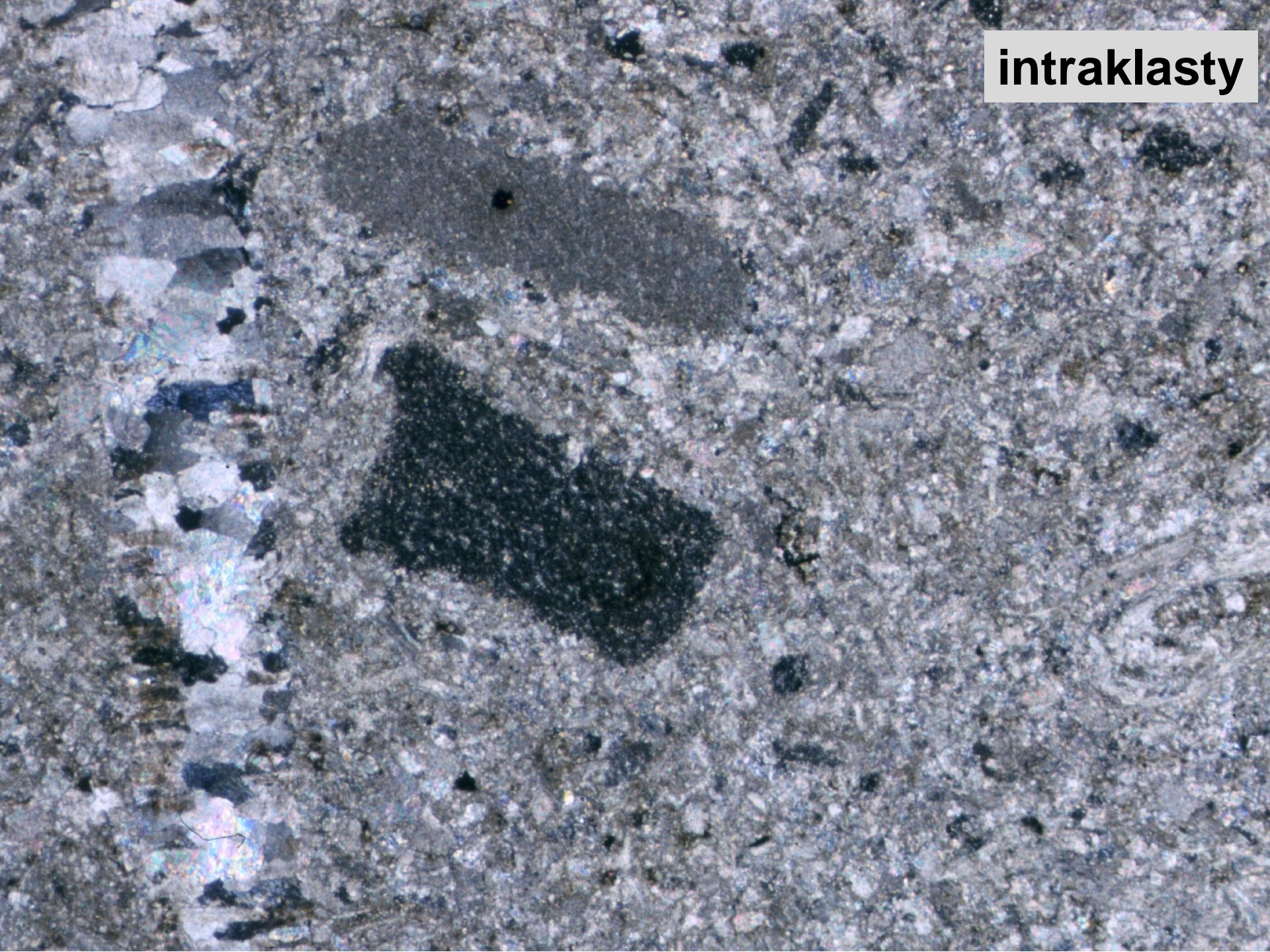
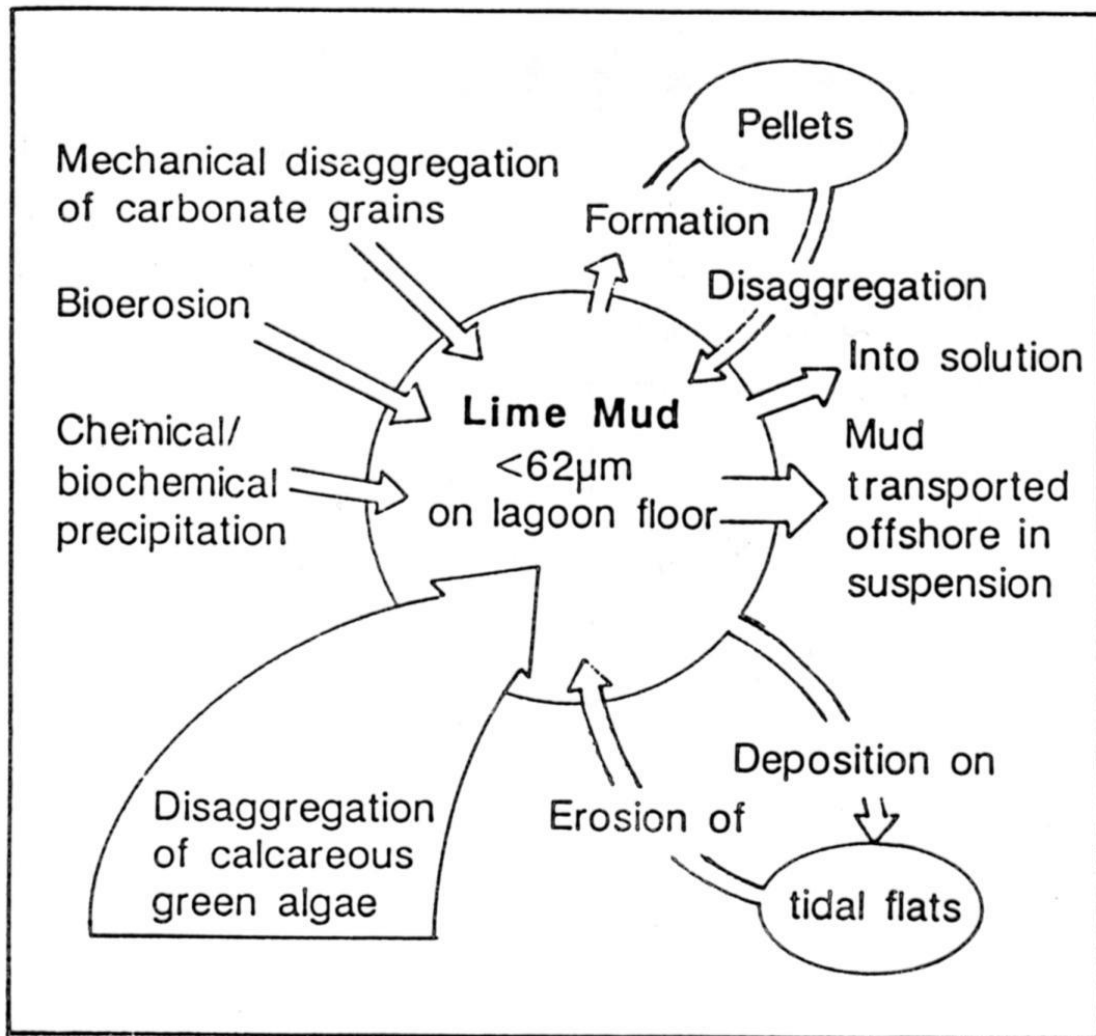


Fig. 4.7 Age range and generalized taxonomic diversity of principal carbonate-secreting organisms. After Horowitz & Potter (1971).

intraklasty





matrix:

mikrit - pod 5 mikrometrů

vápnitý kal – pod 50 (62) mikrometrů

tmel (cement):

sparit – nad 50 mikrometrů

Fig. 1.13 *Lime mud budget for the Bight of Abaco, Bahamas. Based on Neumann & Land (1975) and Tucker (1981).*

Folkova klasifikace (podle složení)

Principal allochems in limestone	Limestone types	
	cemented by sparite	with a micritic matrix
skeletal grains (bioclasts)	biosparite	biomicrite
ooids	oosparite	oomicrite
peloids	pelsparite	pelmicrite
intraclasts	intrasparite	intramicrite
limestone formed in situ	biolithite	fenestral limestone -dismicrite

Fig. 4.35 Classification of limestones based on composition. After Folk (1962).

stromatolity

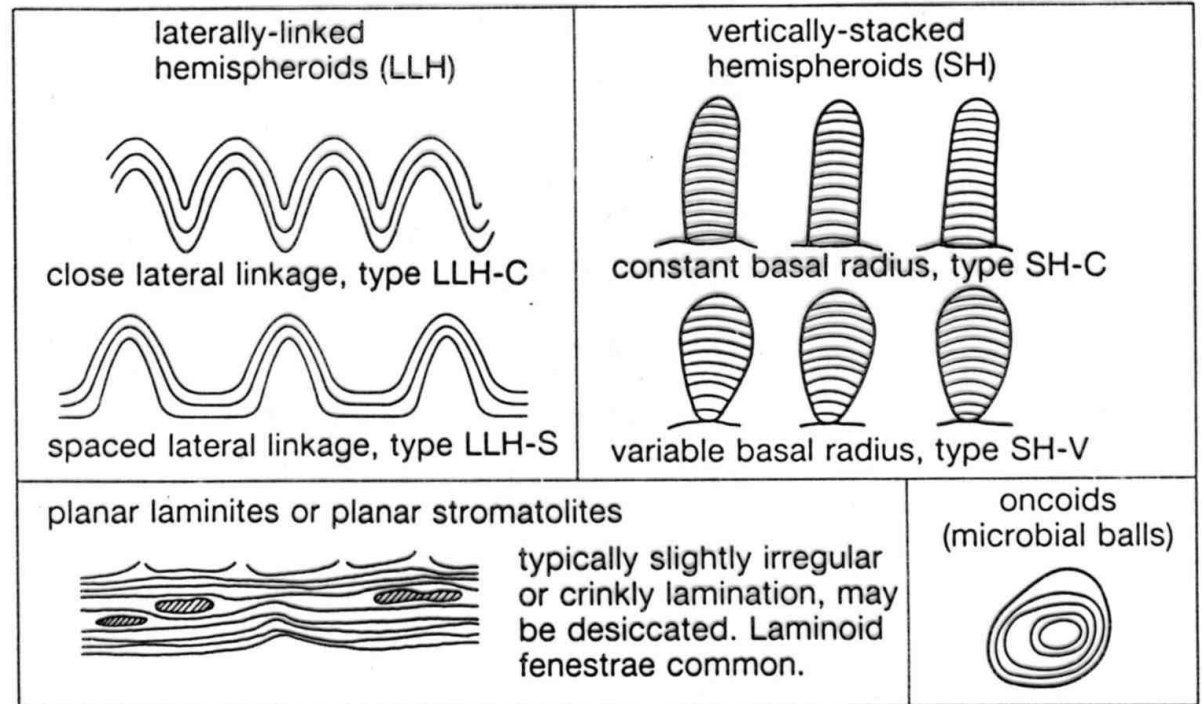


Fig. 4.31 Common types of stromatolite with terminology. After Logan *et al.* (1964).

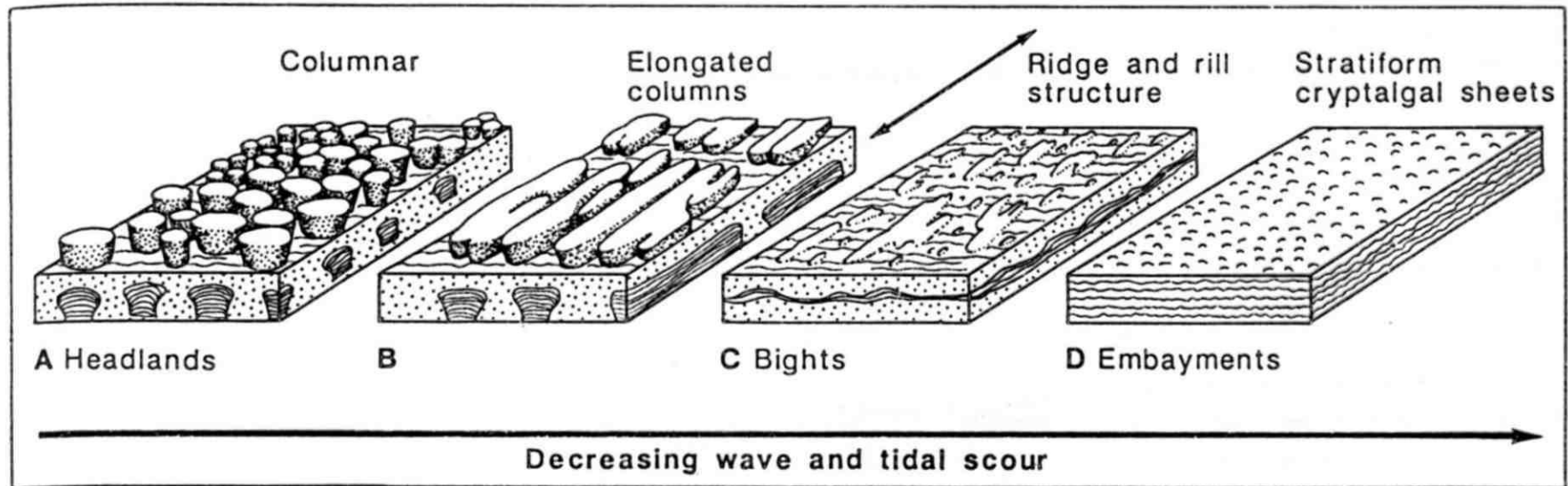


Fig. 4.49 Schematic diagram of the variations in stromatolite form related to wave and tidal scour (modified from Wright, 1984). Discrete columnar forms (A) occur on headlands fully exposed to waves. The relief of the columns is proportional to the intensity of wave action. Elongation of the columns occurs parallel to the direction of wave attack (B) and occurs in less-exposed bights near headlands. In areas partially protected from wave attack, ridge and rill structures develop (C) with relief of 0.1–0.3 m. In small embayments, completely protected from waves, stratiform sheets occur with relief of less than 40 mm (D). These four all represent pustular mat forms from Shark Bay. Based on data in Hoffman (1976). However, Burne & James (1986) have interpreted the intertidal columnar forms as subtidal forms exposed by a drop in sea-level. Similar subtidal forms have been described from tidal channels in the Bahamas by Dill et al. (1986; Fig. 3.12).

struktury

teepee, hardgroundy, paleokras, strukturní klasifikace (Dunham 1962)

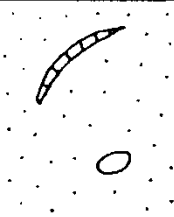
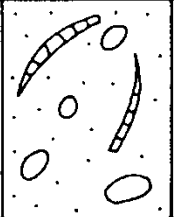
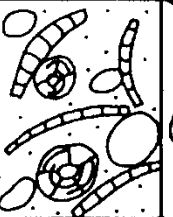
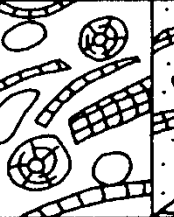

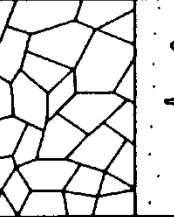





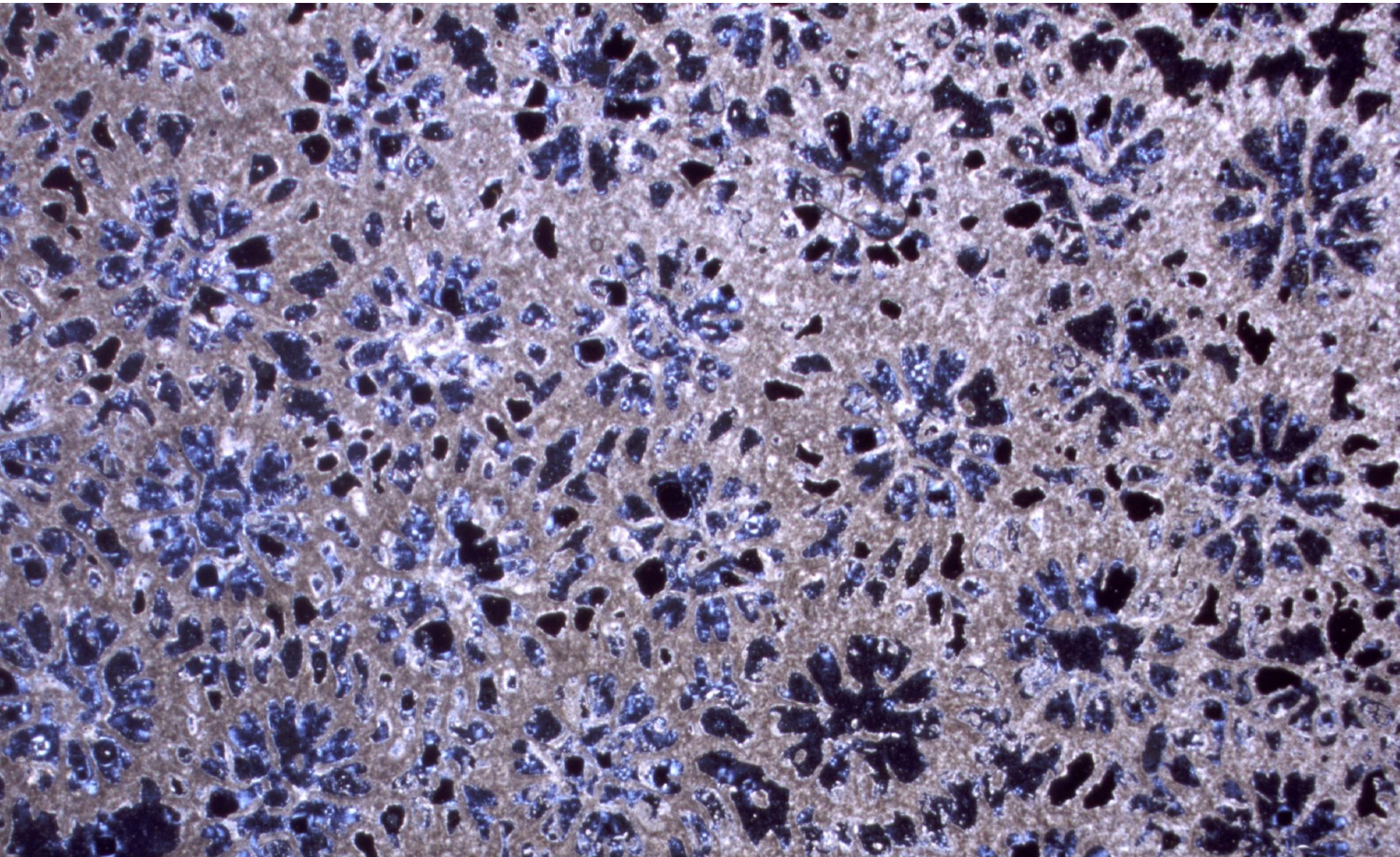
original components not bound together during deposition		original components not bound together	depositional texture not recognizable	original components not organically bound during deposition		original components organically bound during deposition				
contains lime mud				lacks mud and is grain supported	>10% grains >2mm	matrix supported	supported by >2mm component	organisms act as baffles	organisms encrust and bind	organisms build a rigid framework
mud-supported	grain-supported									
less than 10% grains	more than 10% grains									
mudstone	wackest.	packstone	grainstone	bound stone	crystalline	floatstone	rudstone	baffle stone	bindstone	frame stone
										

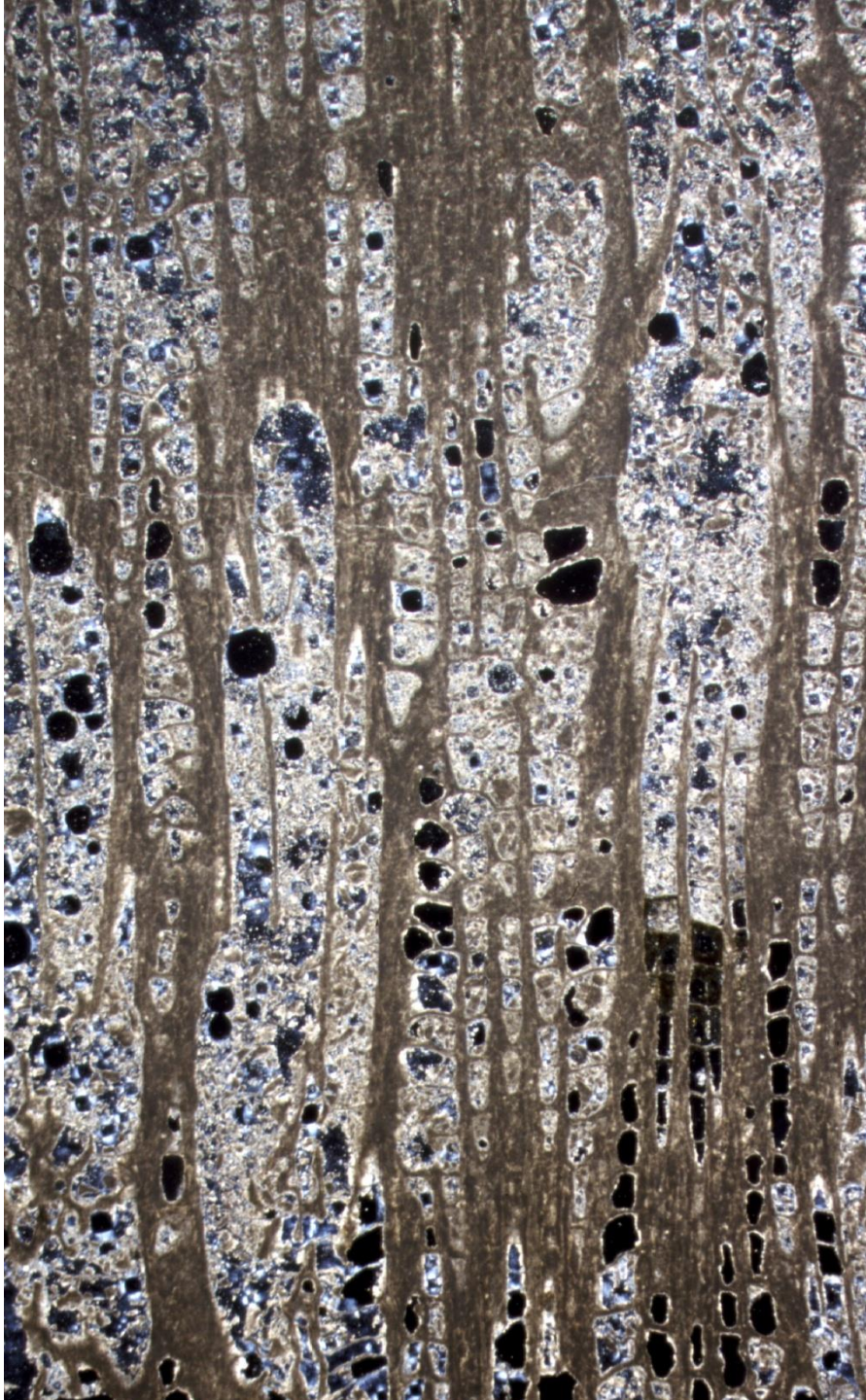
Fig. 4.36 Classification of limestones based on depositional texture. After Dunham (1962) with modifications of Embry & Klovan (1971).

Depositional Texture Classification

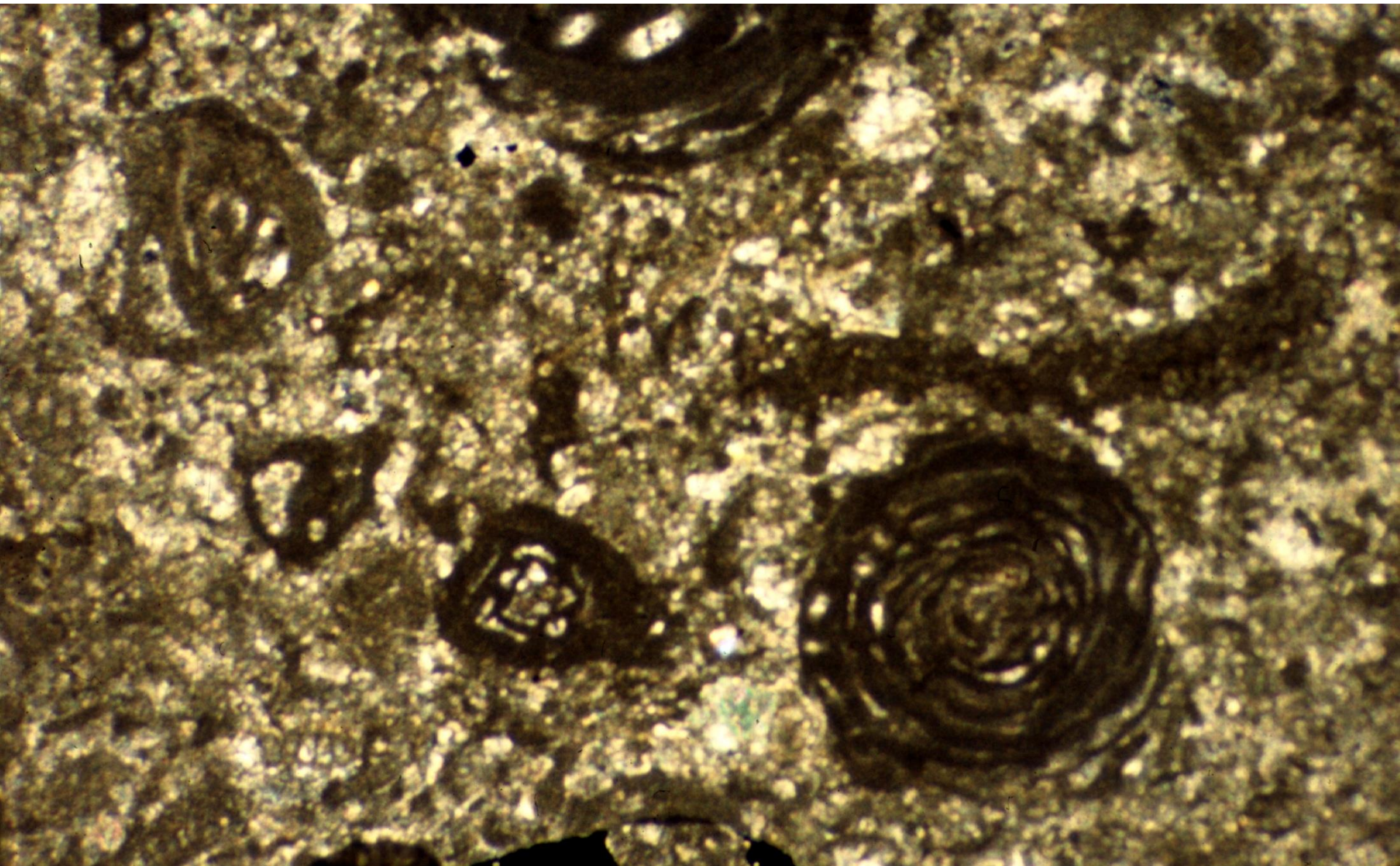
Depositional Texture Recognized				Not Recognizable
Not Bound at Deposition		Bound at Deposition		 <p>CRYSTALLINE CARBONATE</p>
Mud-supported	Grain-supported			
<p>< 10% Grains</p>  <p>MUDSTONE</p>	<p>> 10% Grains</p>  <p>WACKESTONE</p>	<p>> 1% Mud</p>  <p>PACKSTONE</p>	<p>< 1% Mud</p>  <p>GRAINSTONE</p>	
		 <p>BOUNDSTONE</p>		

biolithit (Folk), boundstone (Dunham); pleistocénní korál, Florida, horizontální řez





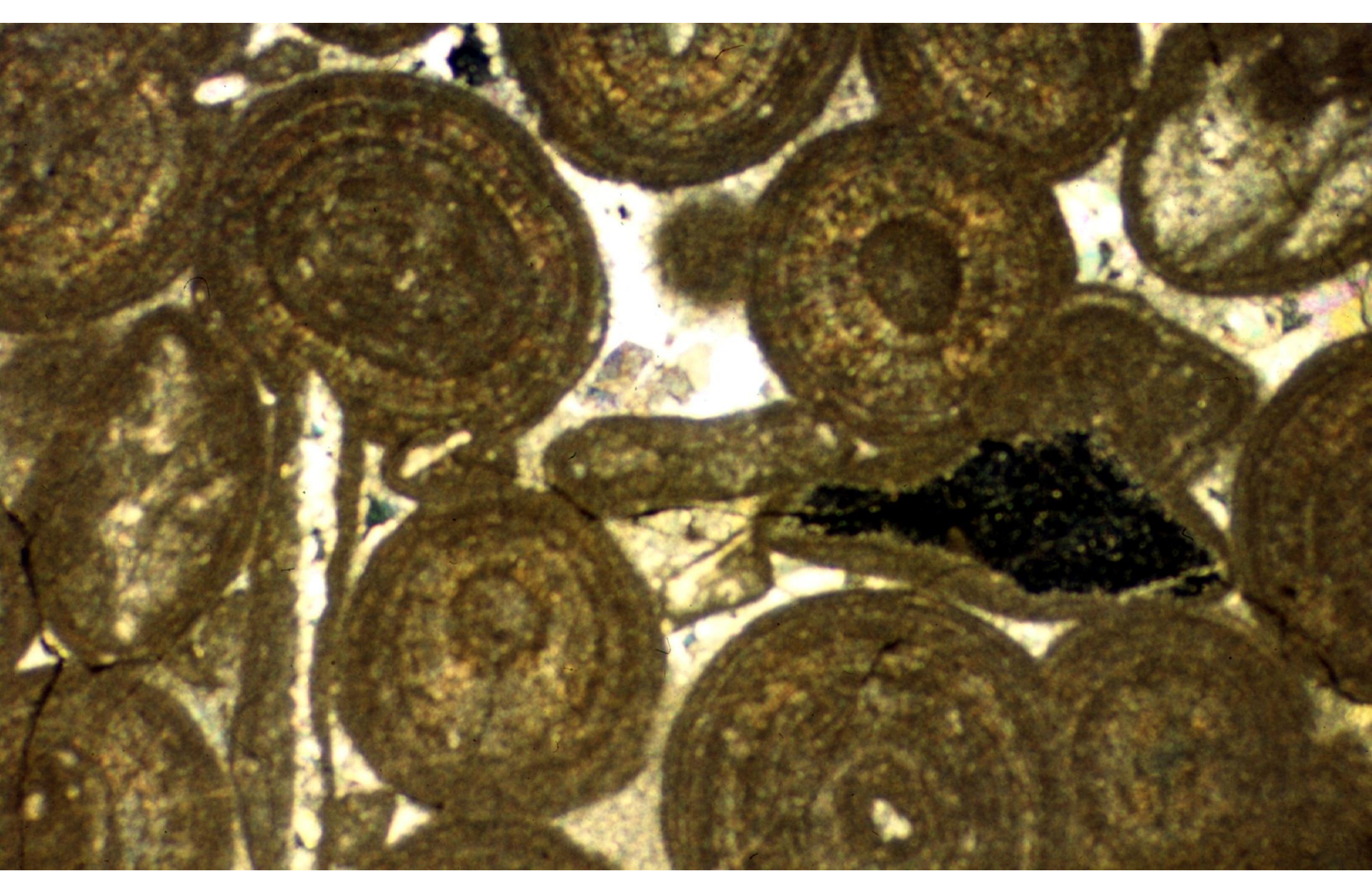
dto
vertikální řez



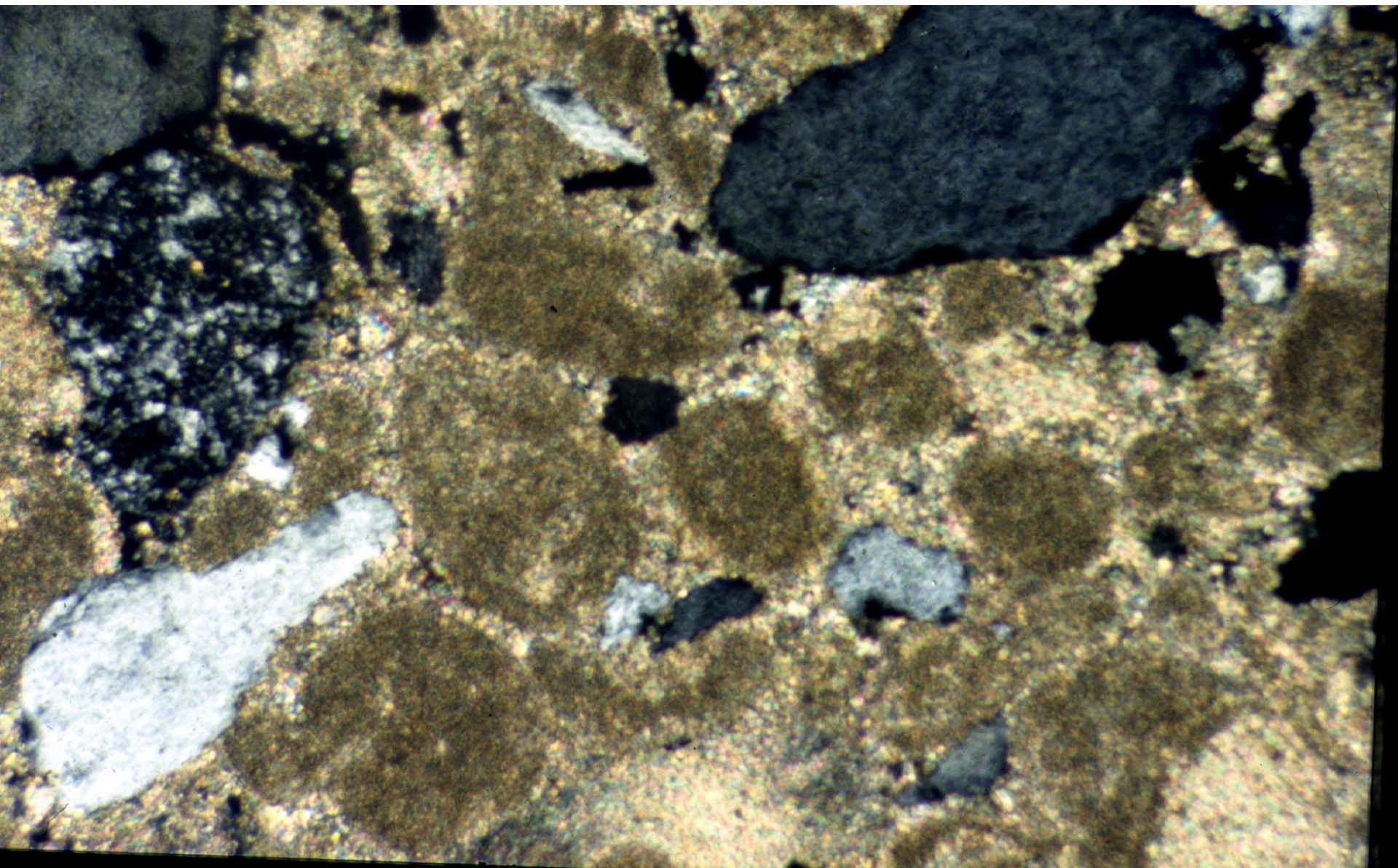
biomikritový wackestone (foraminifery, terciér)



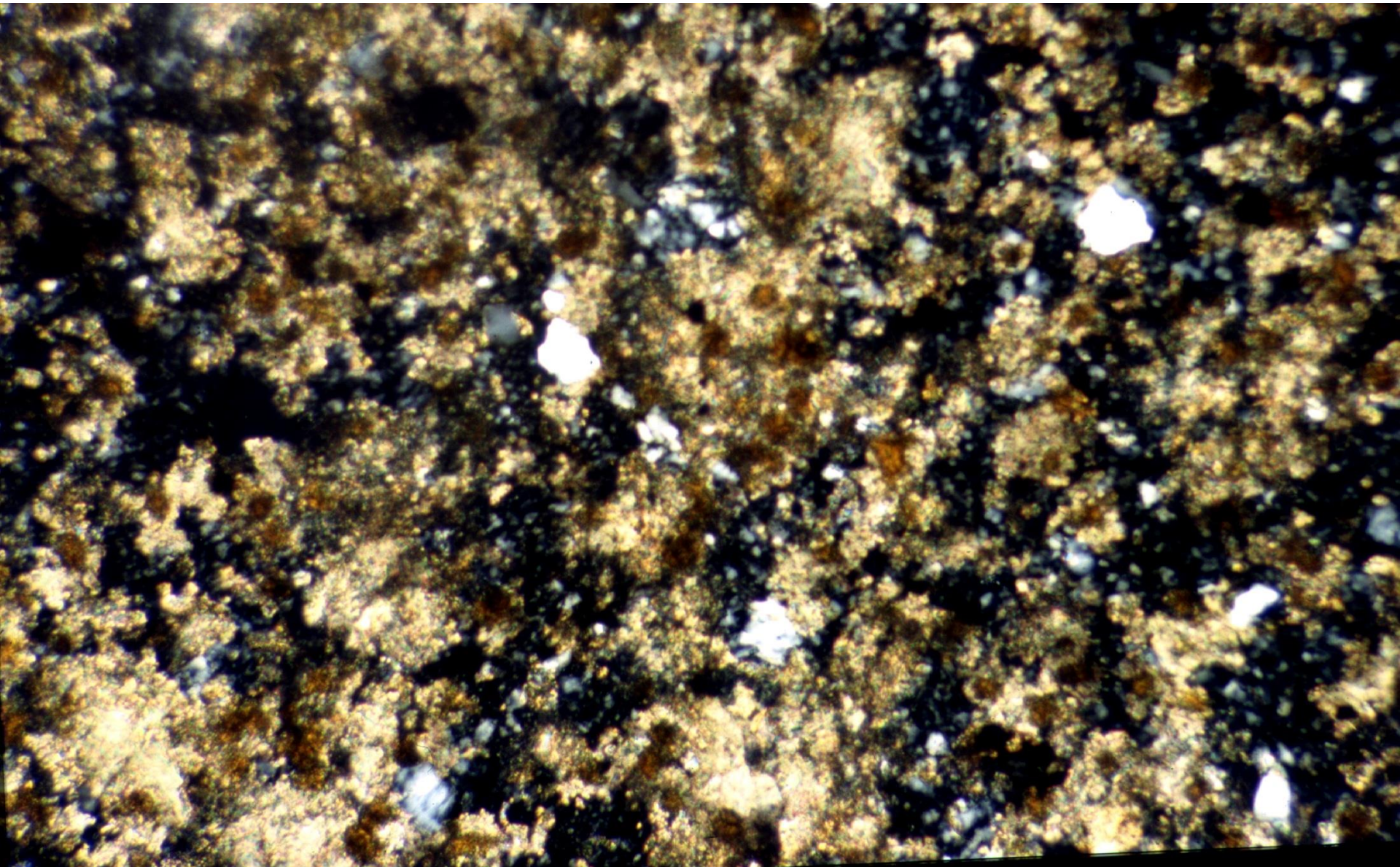
biomikritový packestone (mlži, trilobiti, devon)



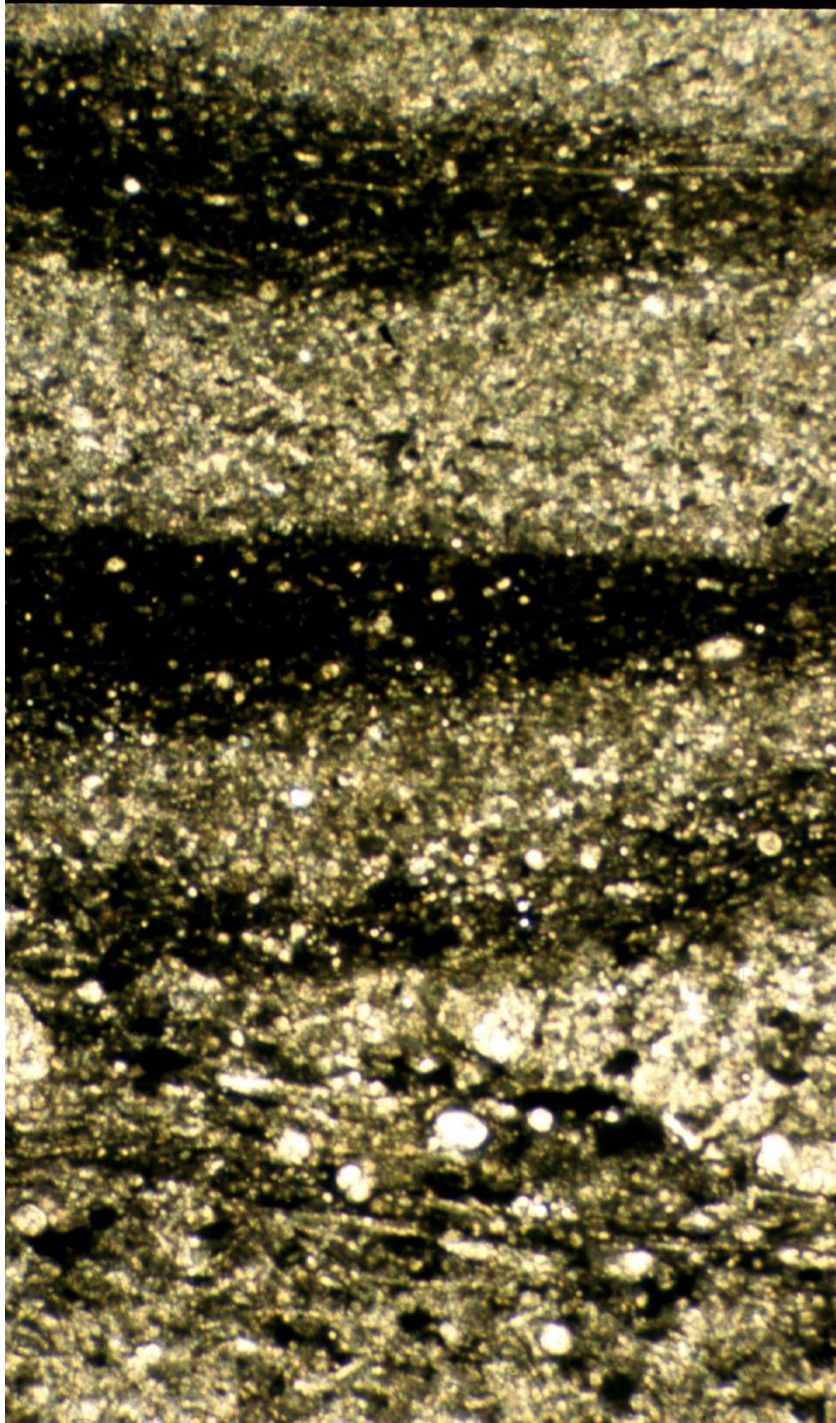
oosparitový grainstone



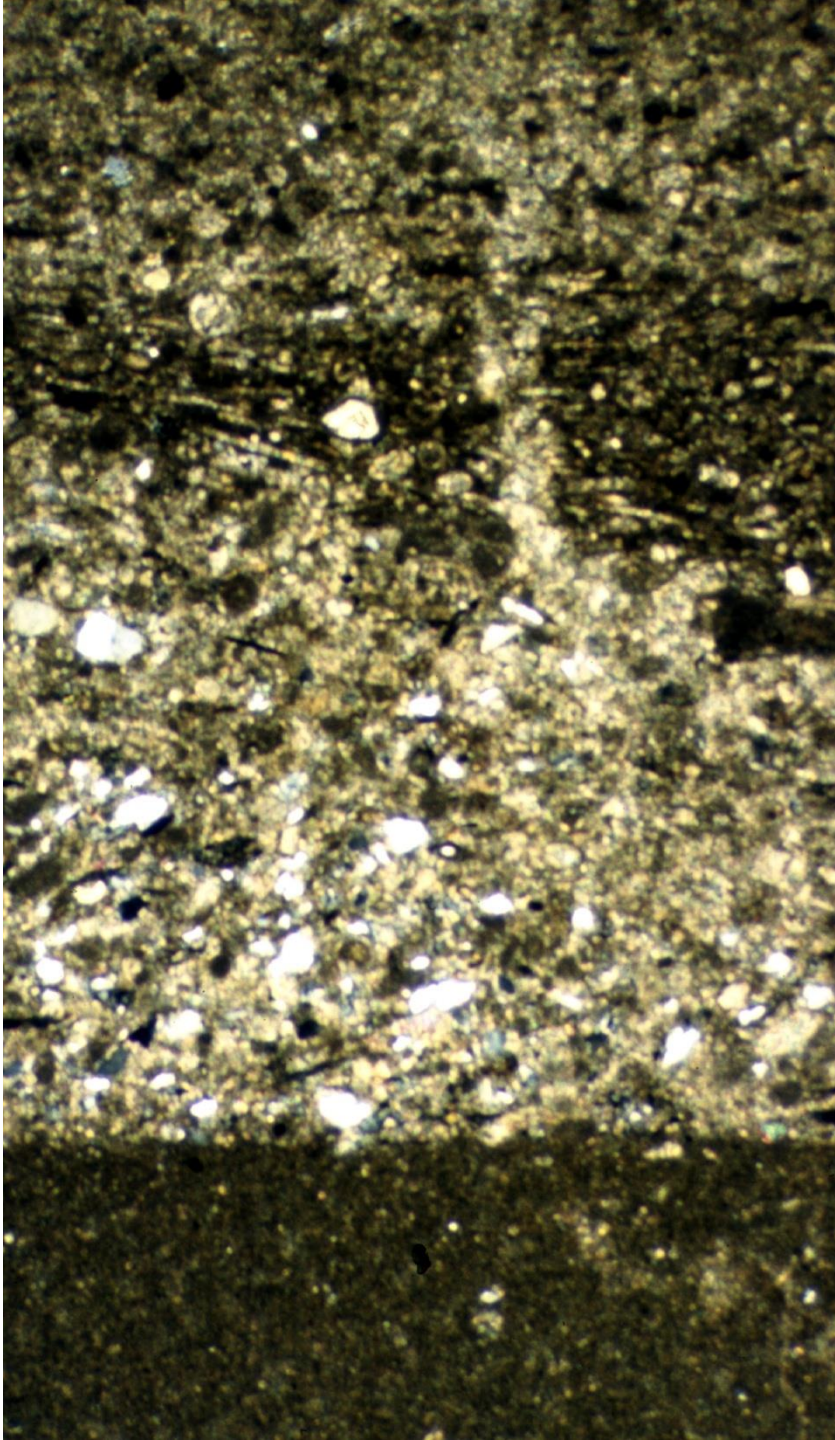
pelmukritový packstone s písčitou příměsí



prachovitý slínovec



mikritový mudstone
laminace



mikritový mudstone
laminace
gradační zvrstvení – distální turbidit

sedimentační prostředí

kontinentální - jezerní, pedogeneze, kalkrusty

mořské - karbonátové platformy:

- hrazený šelf (biohermy, karb. útesy)

- rampy

intertidál - supratidál

lagunární karbonáty

intertidál - subtidál, písčité tělesa

karbonátový šelf

pelagické – CCD

cykličnost (souhra klimatických, tektonických a eustatických změn;
autocykličnost)

Milankovičovy cykly

kontinentální

- eolické
- pedogenní (kalkrusty)
- jezerní
 - aridní, semiaridní – evaporace, chemická precipitace
 - humidní – biochemická, biogenní precipitace karbonátů

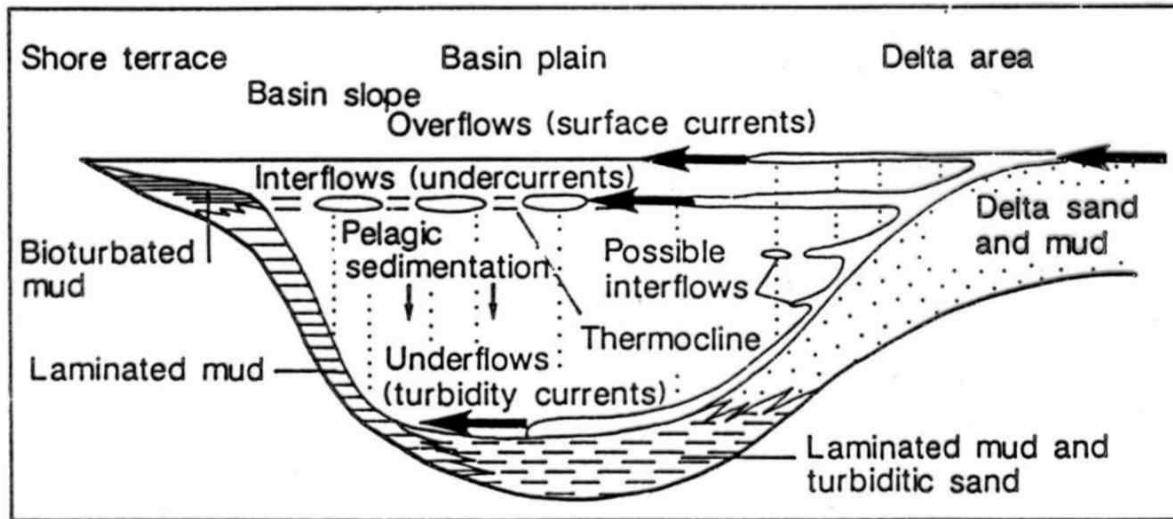


Fig. 4.65 *Sediment dispersal mechanisms and lithofacies for an oligotrophic lake with annual thermal stratification. Based on Sturm & Matter (1978).*

sezónní laminace

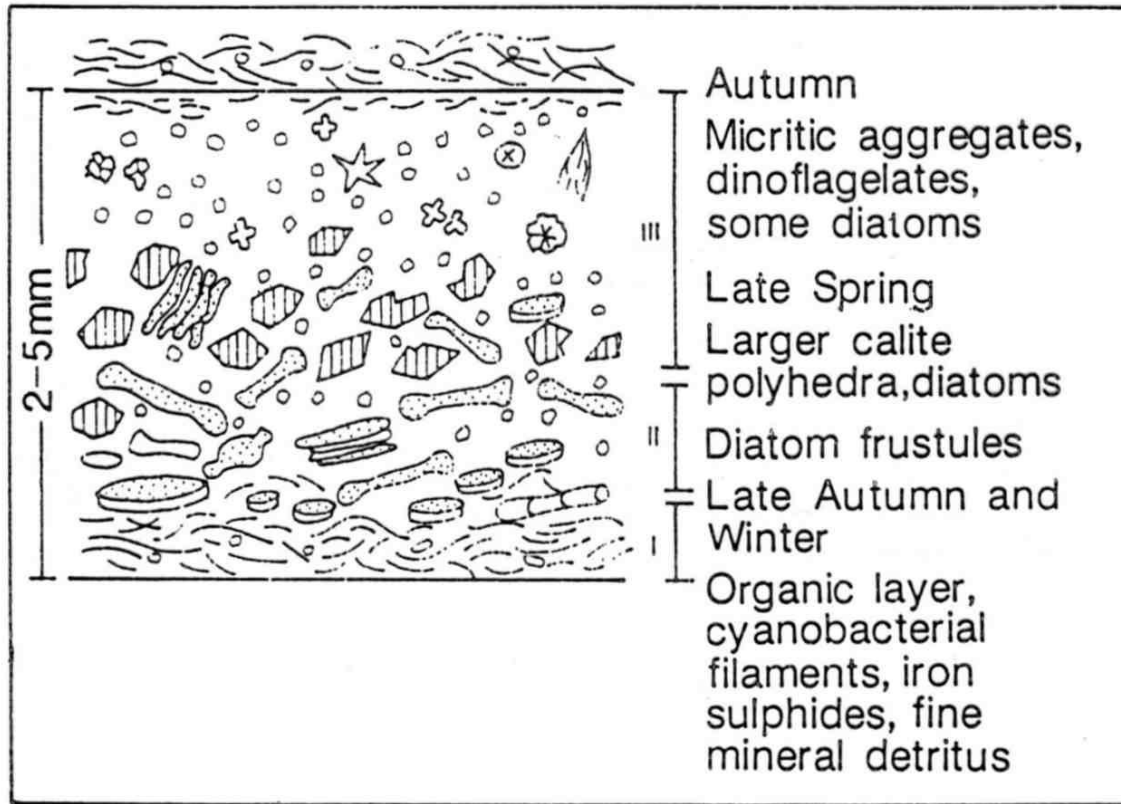


Fig. 4.72 Schematic diagram showing the composition of a triplet from Lake Zurich, Switzerland. Layer I represents settle out from the lake waters. Much of layer II represents diatom blooms. The decreasing crystal size of calcite in layer III reflects changing saturation levels. Modified from Kelts & Hsü (1978); Allen & Collinson (1986).



Figure 20—Low-angle wedge-planar cross beds, Pleistocene eolianite, Isla Contoy, Yucatan Peninsula. Photo by W. C. Ward.

kalkreta

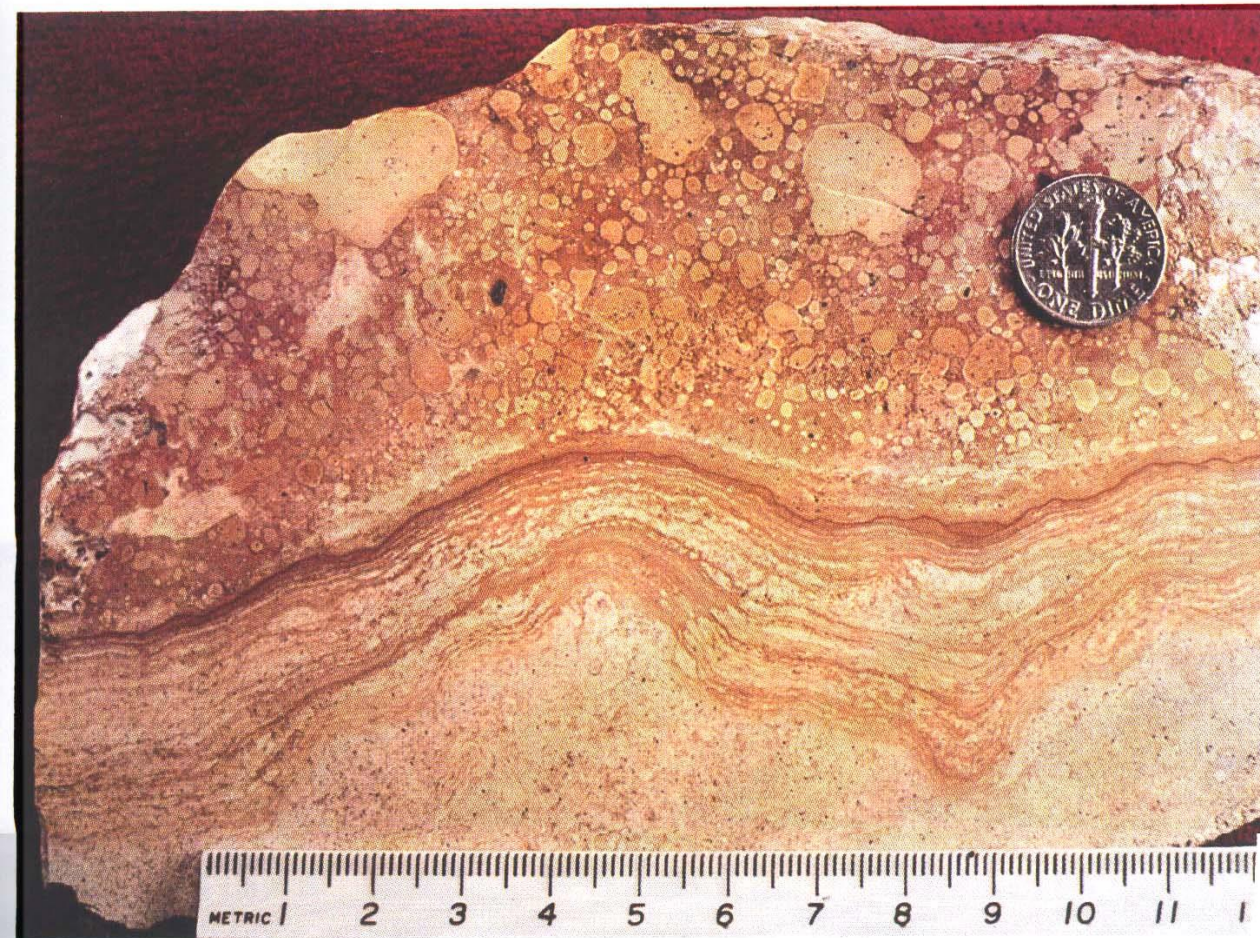


Figure 38—Caliche layers developed on Pleistocene eolianite, Isla Mujeres off the Yucatan Peninsula. Micritized eolianite is overlain by wavy, laminated crust, which is overlain by conglomeratic layer with crude reverse-graded bedding. Photo by W. C. Ward.

mořské - karbonátové platformy: hrazený šelf (biohermy, karb. útesy), rampy

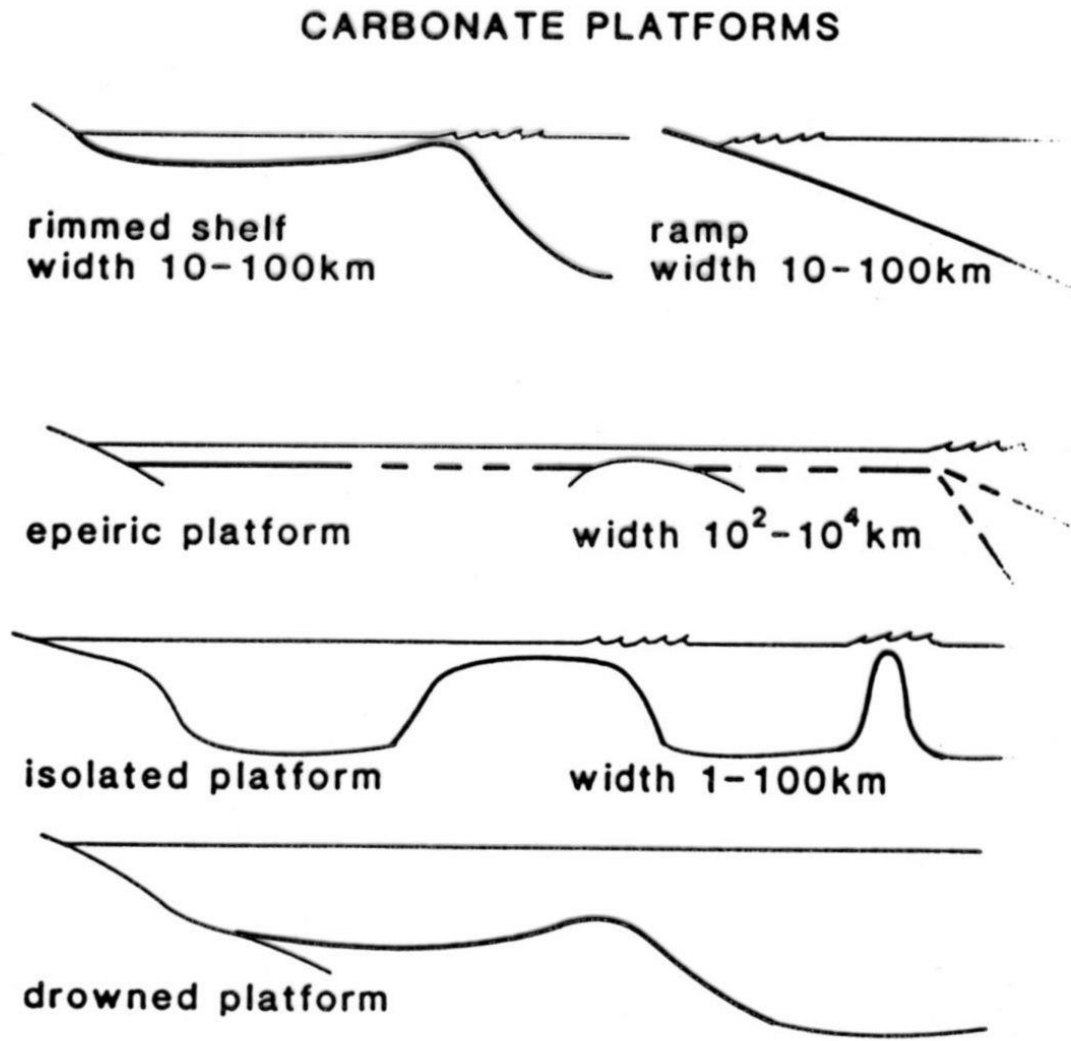


Fig. 4.70 Different types of carbonate platform. After Tucker & Wright (1990).

hrozený šelf (bariéra: karbonátový útes nebo písčité bariéra)

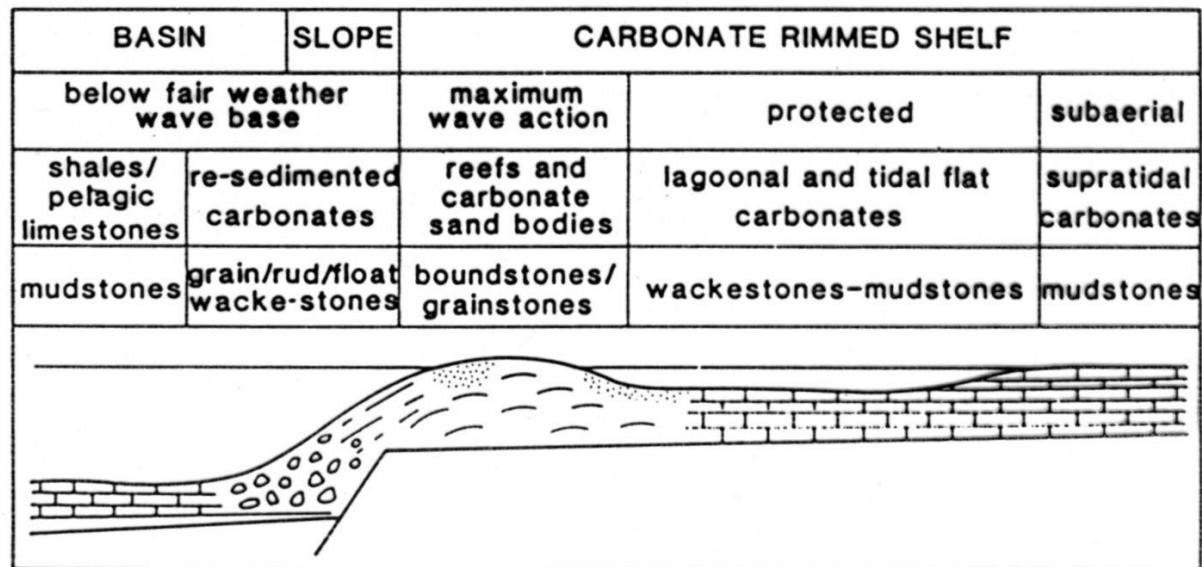


Fig. 4.71 General facies model and limestone types for a rimmed shelf.

karbonátová rampa

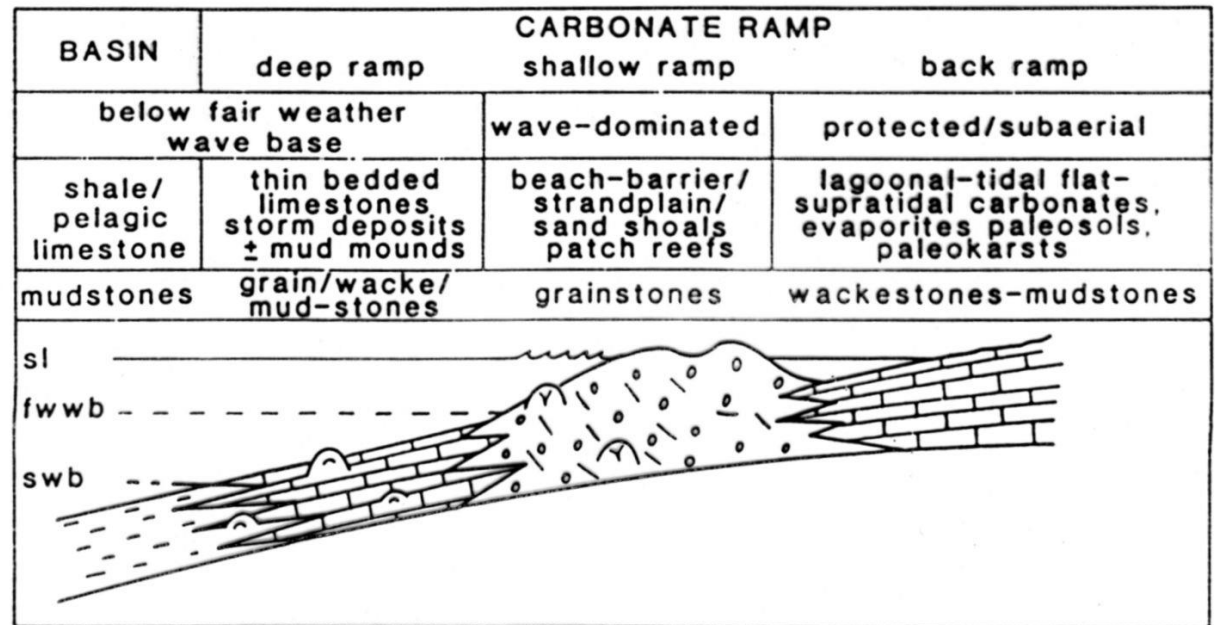


Fig. 4.72 General facies model and limestone types for a carbonate ramp.

karbonátový útes

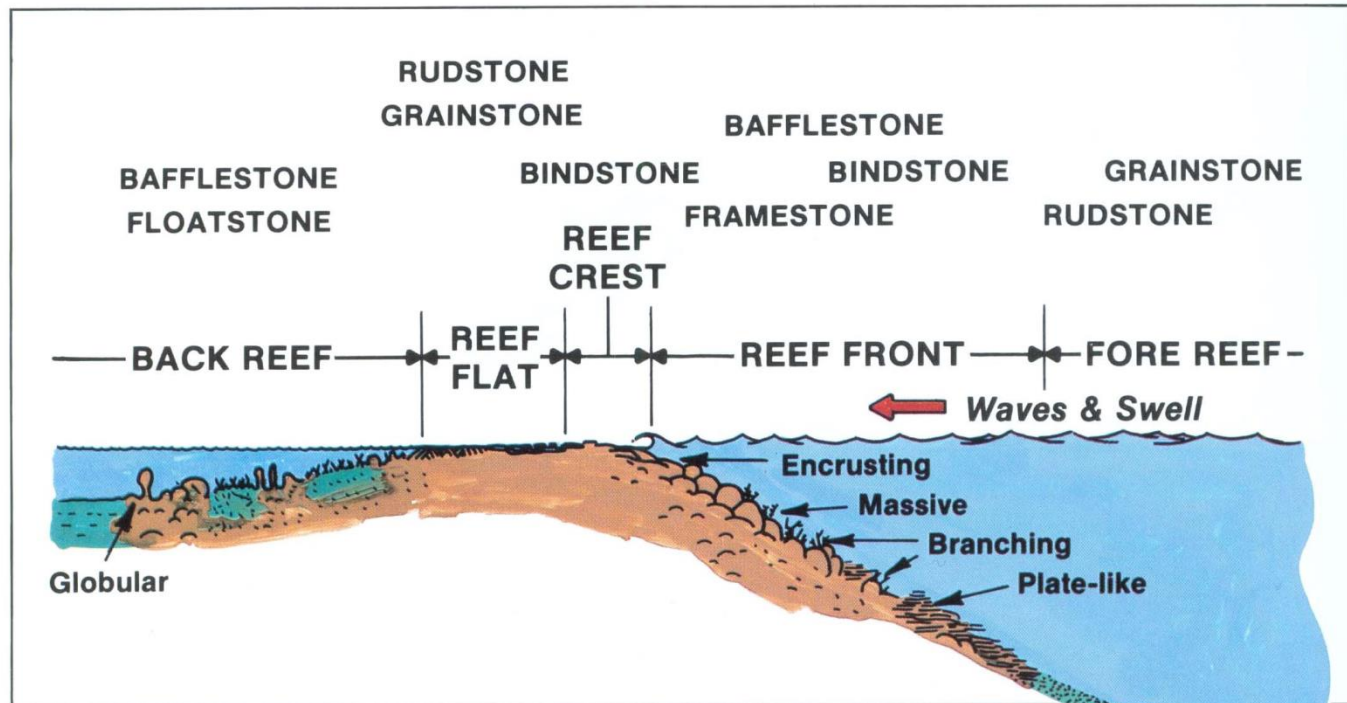
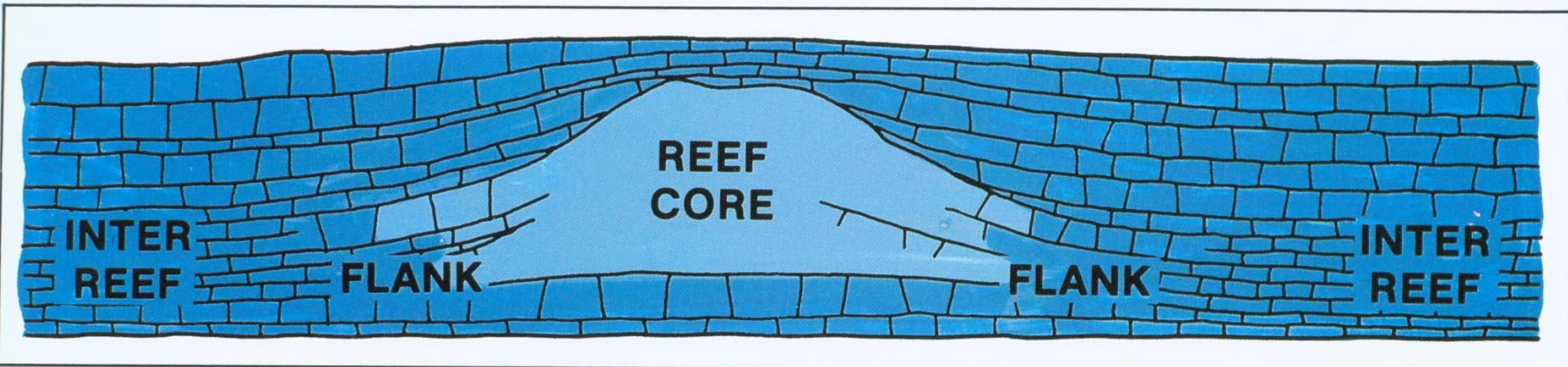


Figure 14—A cross-section through a zoned marginal reef illustrating the different reef zones, spectrum of different limestones produced in each zone, and environment of different reef-building organisms. In many modern reefs, the reef crest is occupied by the massive branching coral *Acropora palmata*, a situation that is rare in the fossil record (after James, 1979, with permission of Geol. Assoc. Canada).

Figure 15—An areal view looking north along the Belize barrier reef on a calm day. The reef crest is the sharp dark line curving toward the upper right with deep water to the lower right. The wide, light-green area shelfward of the very narrow reef crest is a 1 to 2 km wide blanket of skeletal sand (mostly *Halimeda*) with zones of coral rubble in the lee of the reef crest. Passes through the barrier (upper right) are as much as 20 m deep. Numerous patch reefs can be seen on the shelf behind (upper left). (Photo R. N. Ginsburg).







DEPOSITIONAL MARGIN SHALLOW WATER REEF

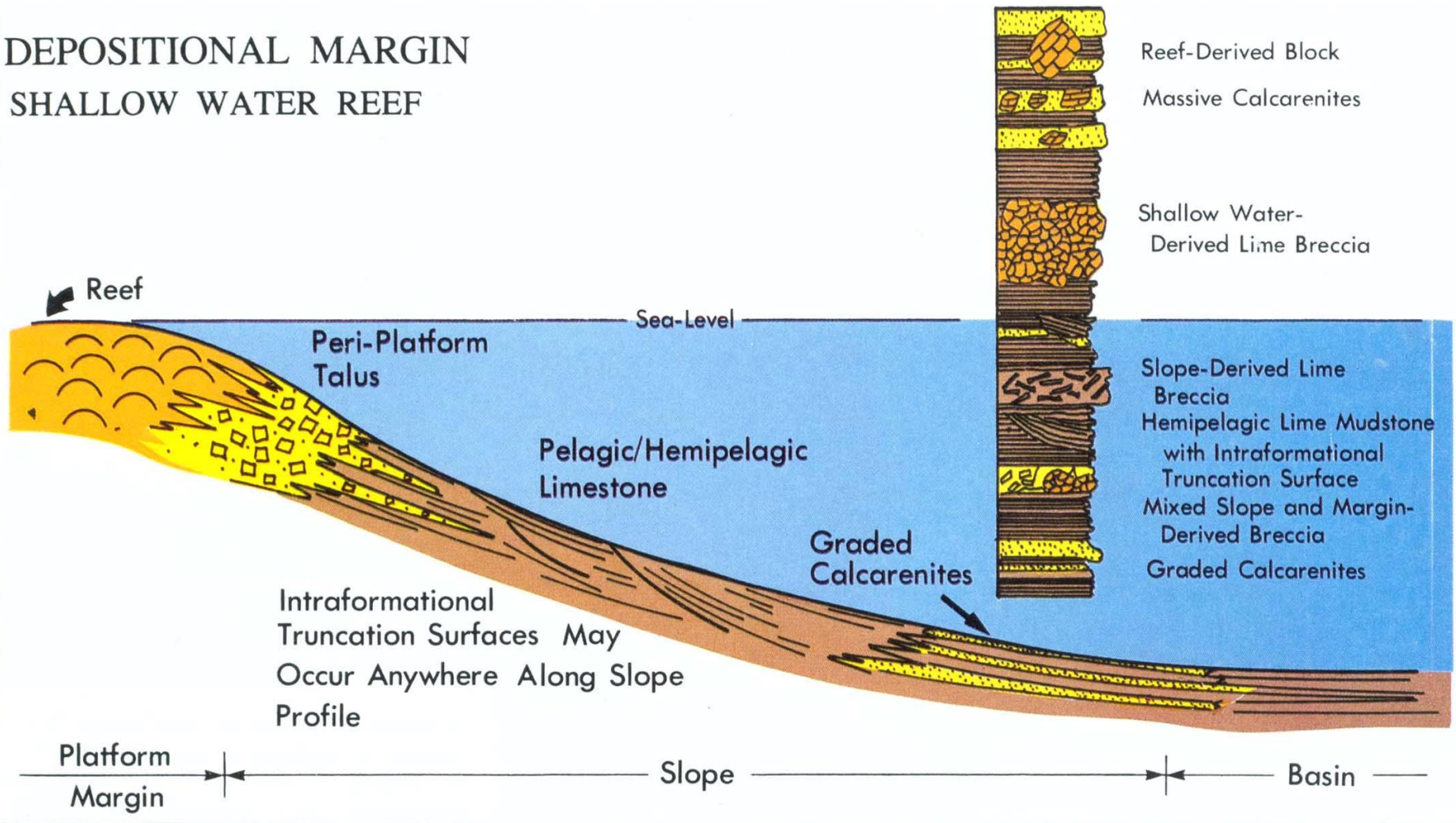


Figure 27—Slope models from McIlreath and James (1978). **A.** (above) Schematic model for a shallow-water, reef dominated, depositional carbonate margin, and illustration of a hypothetical sequence of deposits from slope accretion. **B.** (facing page) Schematic model for a shallow-water, reef dominated, bypass type of carbonate margin.

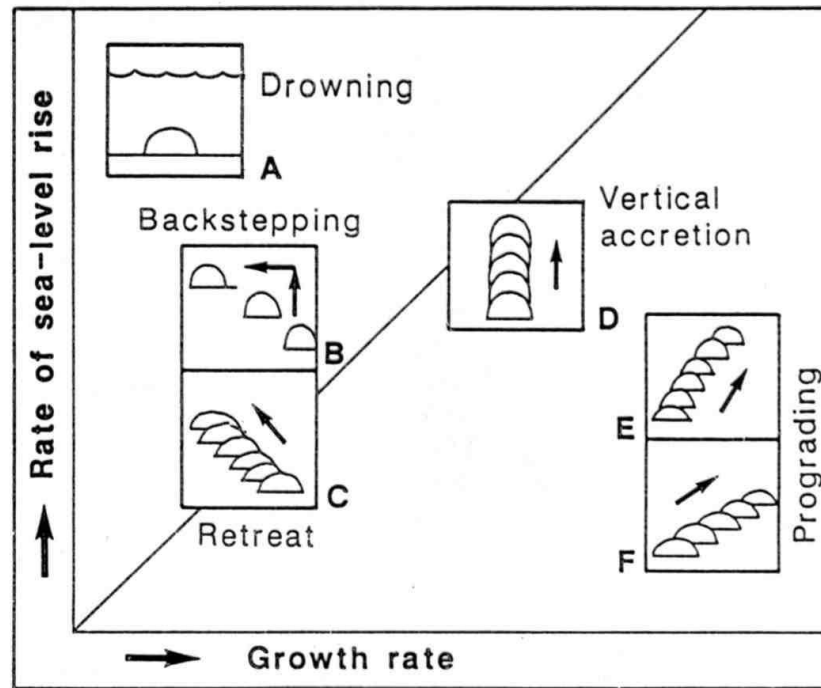


Fig. 4.97 Schematic diagram showing the responses of reefs to sea-level rise. Growth rate refers to the actual accretionary rate of the reef and not to the biological growth rate. In (A), the rate of sea-level rise greatly exceeds the reef growth rate, and the reef is drowned below the depths of biological growth. In (B), the rate of sea-level rise is pulsed allowing recolonization but in progressively shallower waters (backstepped) (Figs 4.98 and 4.99). In (C), the rate of sea-level rise is nearly balanced by accretion and the reef retreats into shallow water. In (D), accretion and sea-level rise are balanced and vertical accretion occurs. In (E) and (F) the rate of sea-level rise is slow enough for the reef to prograde into deeper water (Fig. 4.100). These geometries relate to reefs on shelf or platform edges but isolated reef complexes will show such responses on all sides, although to varying degrees.

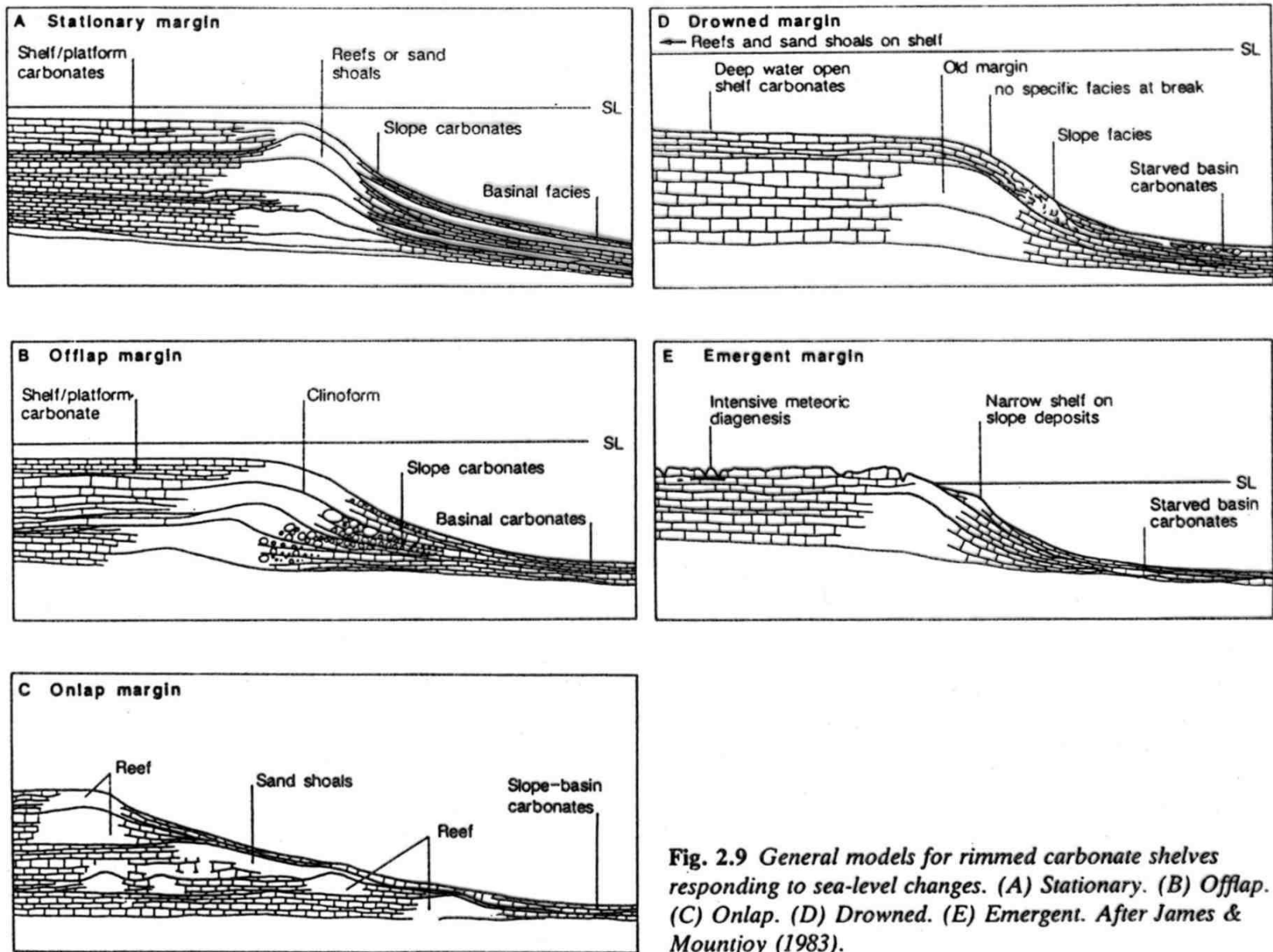


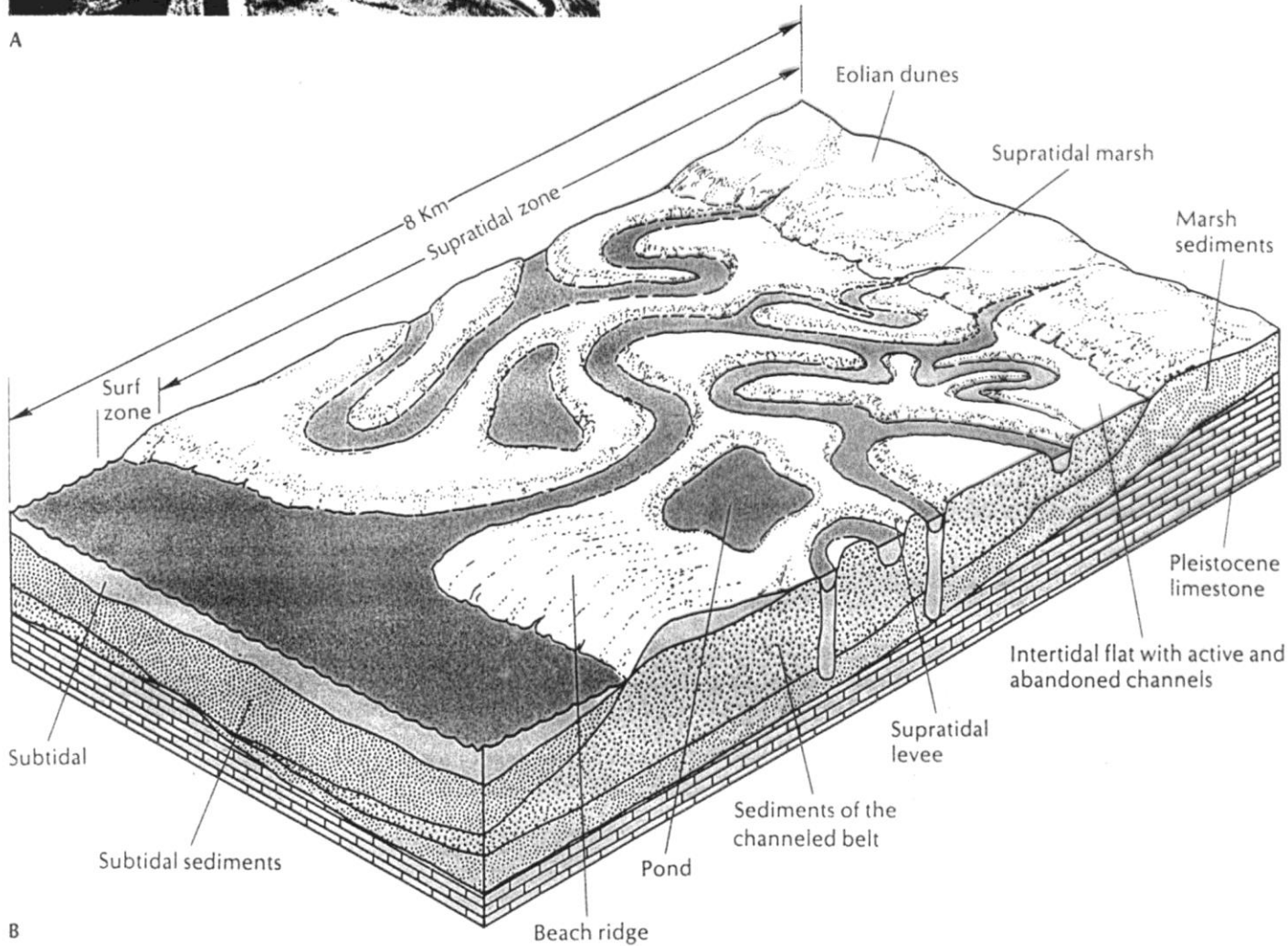
Fig. 2.9 General models for rimmed carbonate shelves responding to sea-level changes. (A) Stationary. (B) Offlap. (C) Onlap. (D) Drowned. (E) Emergent. After James & Mountjoy (1983).



Figure 6.2

(A) The Three Creeks area along the west coast of Andros Island, Bahamas; tidal channels cut an intertidal marsh composed largely of algae, with some ponds in the intertidal areas. (B) Diagram showing major features of the peritidal environment. From Stanley (1989).

intertidál - supratidál



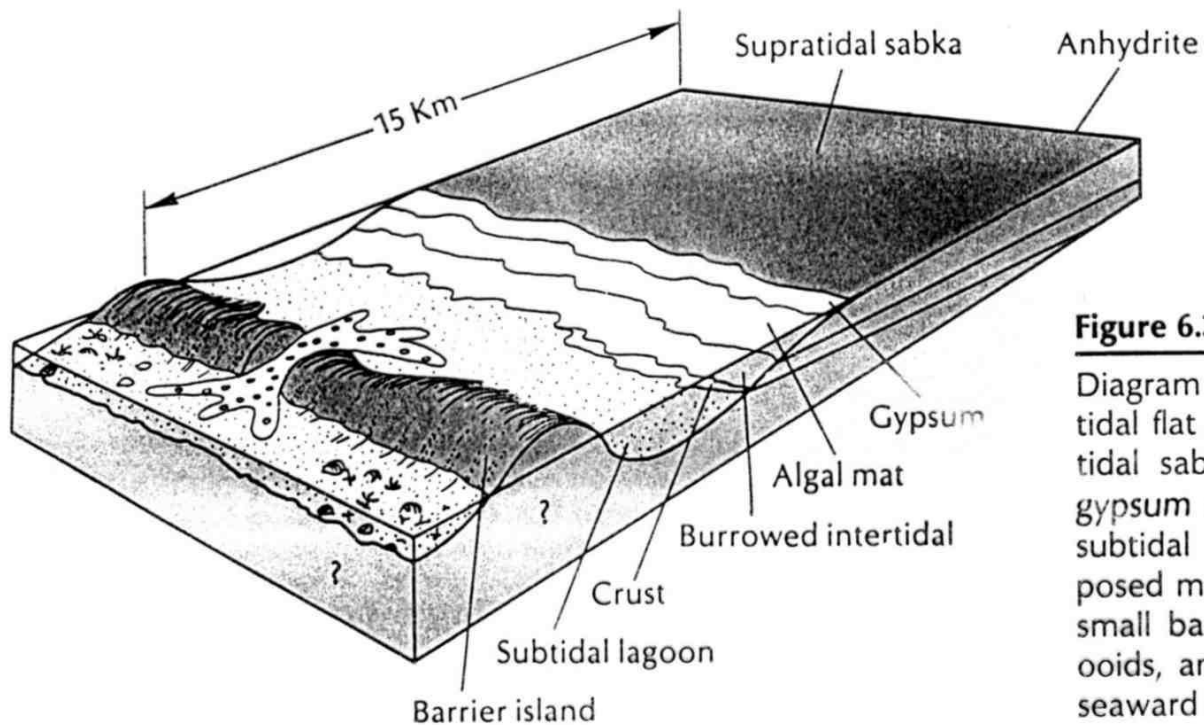


Figure 6.3

Diagram showing the major facies of the regressive tidal flat on the Persian Gulf Trucial Coast. Supratidal sabkha is composed of algal mats with a gypsum crust, which have grown over burrowed subtidal lagoonal sediments. Tidal deltas, composed mainly of ooids, form around inlets cut into small barrier islands composed of mollusc shells, ooids, and coral fragments. Coral reefs can grow seaward of the island, away from the tidal inlets.

lagunární/peritidální karbonáty

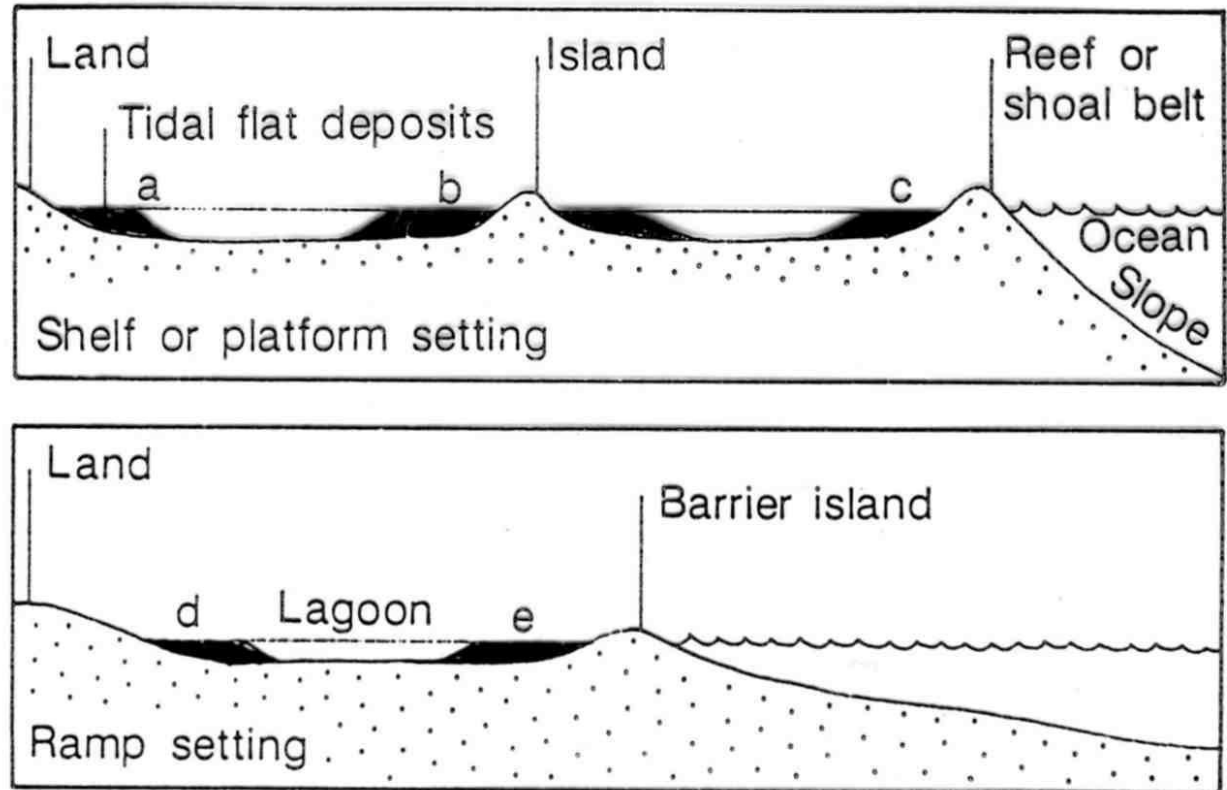
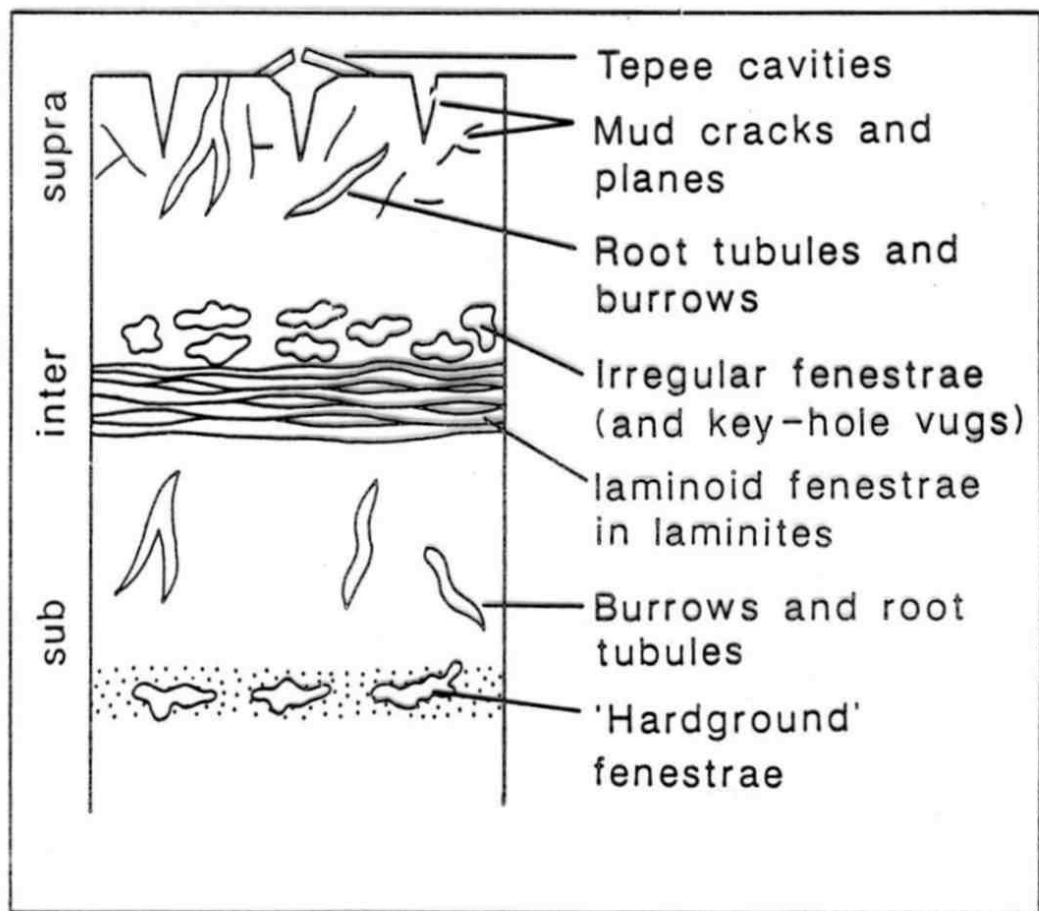


Fig. 4.39 Sites of tidal flat deposition on shelves/platforms and ramps. Examples: (a) Florida Bay; (b) shelf islands of Belize (Ebanks, 1975) and Lower Ordovician of Newfoundland (Pratt & James, 1986); (c) Andros Island, Bahamas (Chapter 3); (d) and (e) Trucial Coast of Arabian Gulf.



sedimentární struktury
v peritidálním
prostředí

Fig. 4.47 *Open-space structures in peritidal deposits (see text). Planes are fractures, and is a term used by soil scientists for open cracks.*

karbonátový šelf

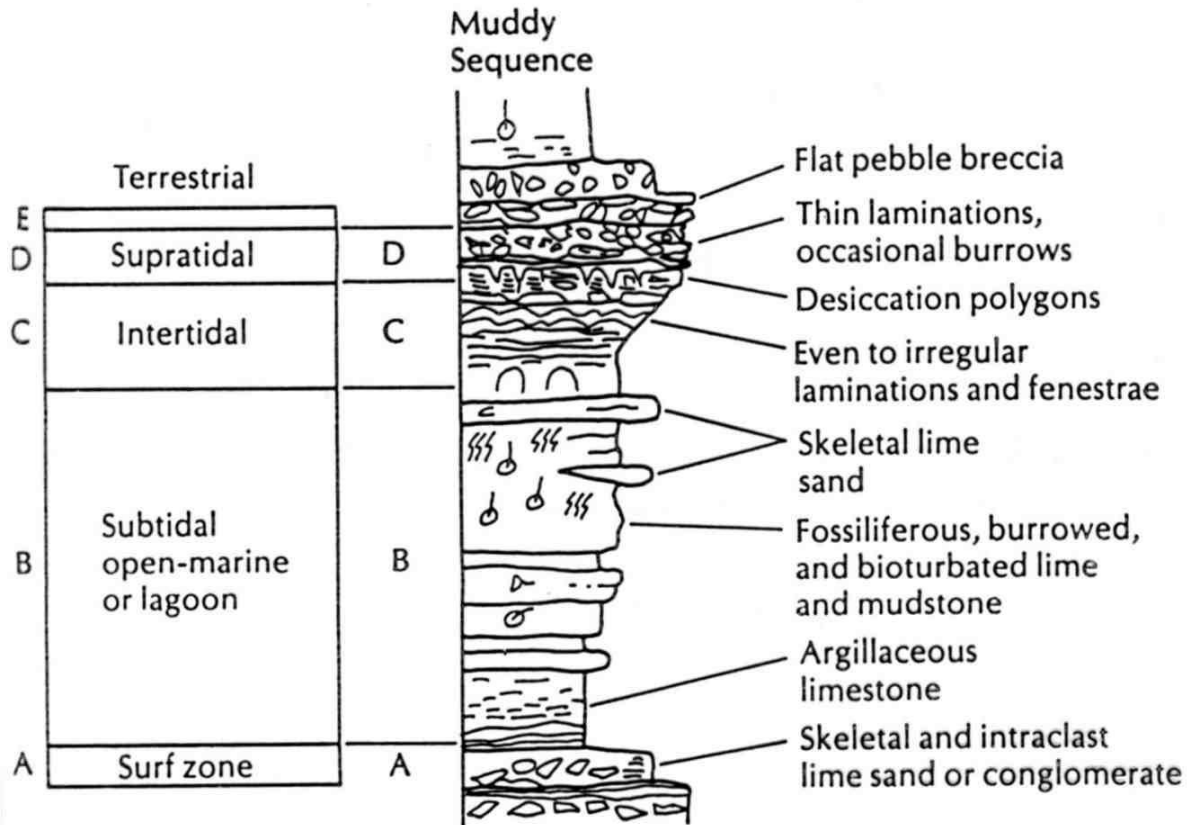
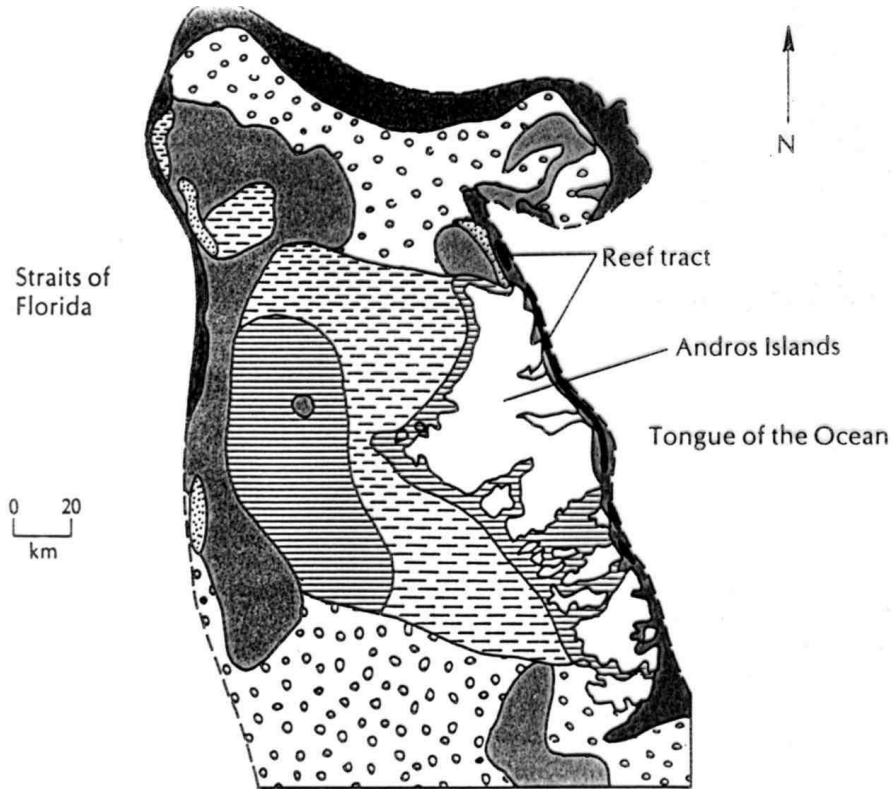


Figure 6.13

Hypothetical shallowing-upward sequence on a low-energy carbonate shelf. From James (1984).

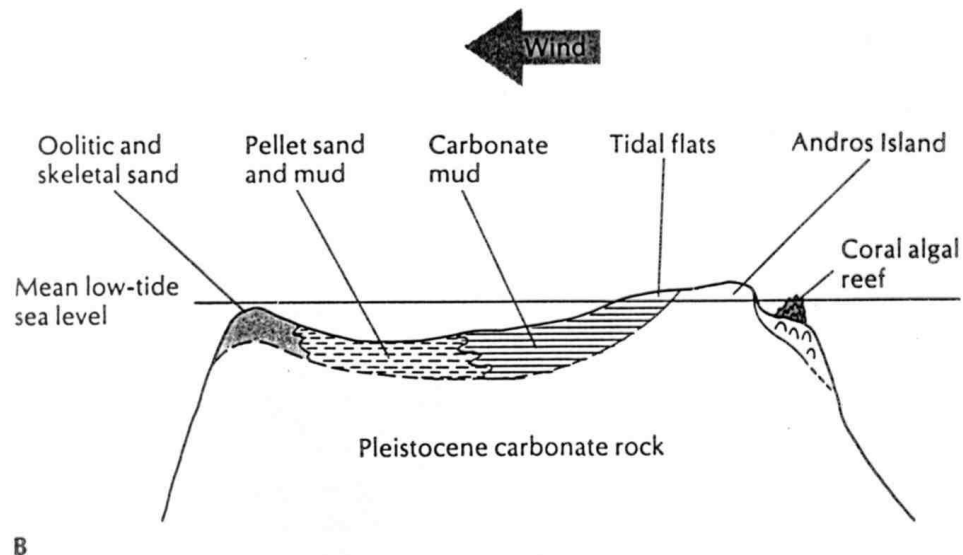


A

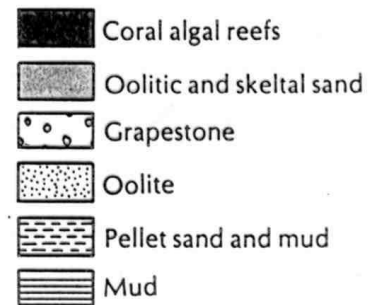
role větru, vlnění a
morfologie při distribuci
mělkovodních
karbonátových facií

Figure 6.10

(A) Generalized map of the carbonate facies of the Bahama Banks near Andros Island. From Sellwood (1978). (B) Cross section of the Bahamas Banks, showing principal facies. From Blatt et al. (1980).



B



pelagické karbonáty – kalcitová kompenzační hladina CCD
 aragonitová kompenzační hladina ACD

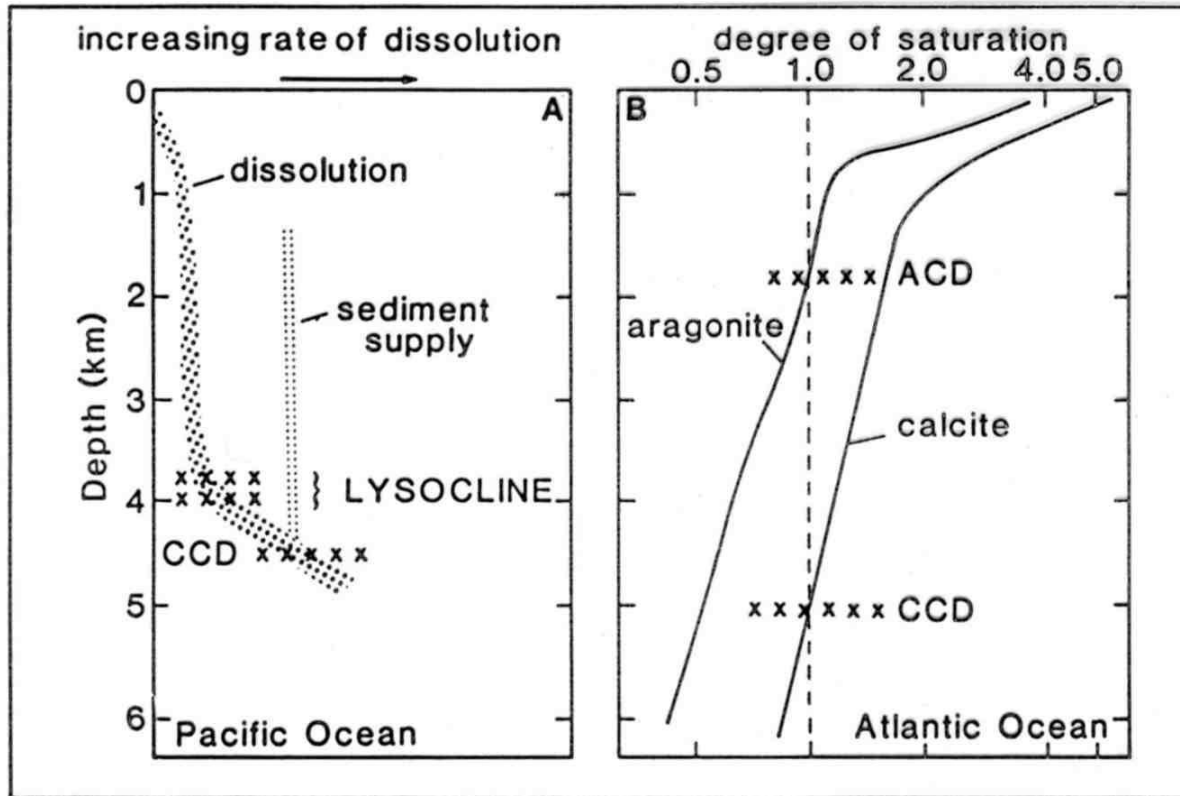
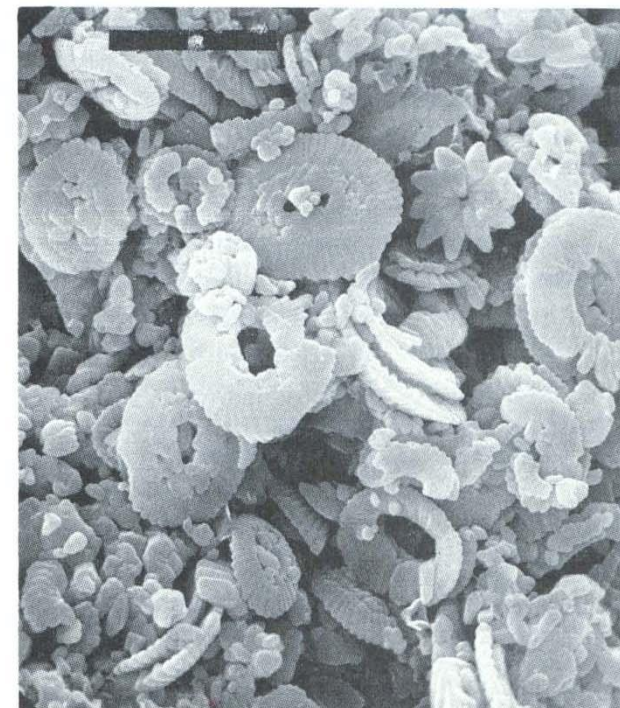


Fig. 5.1 Carbonate saturation and dissolution in the deep sea. (A) The profile of increasing CaCO_3 dissolution with increasing depth for the Pacific Ocean. The lysocline is the depth where the rate of dissolution increases markedly, and the CCD is the depth where the rate of sediment supply is matched by the rate of dissolution and below which therefore the sediments are CaCO_3 -free. After Jenkyns (1986). (B) The profiles of decreasing degree of saturation for aragonite and for calcite with increasing depth for the Atlantic Ocean. After Scholle et al. (1983).



Figure 13—**A.** (left) Scanning electron microscope (SEM) photograph of epicon-tinental shelf chalk from Smokey Hill Shale Member of the Niobrara Formation. Sample shows well preserved, varied assemblage of coccoliths and rhabdoliths and porosity in the 35 to 40% range; scale bar is 10 μm . **B.** (below) SEM photograph of typical Tertiary deep-sea chalk from the Hatton-Rockall Basin. Note minor corrosion of coccolith margins. DSDP Leg 12, Site 116 at 462-m burial depth. Scale bar is 4.5 μm .



cykličnost v
sedimentárním
záznamu

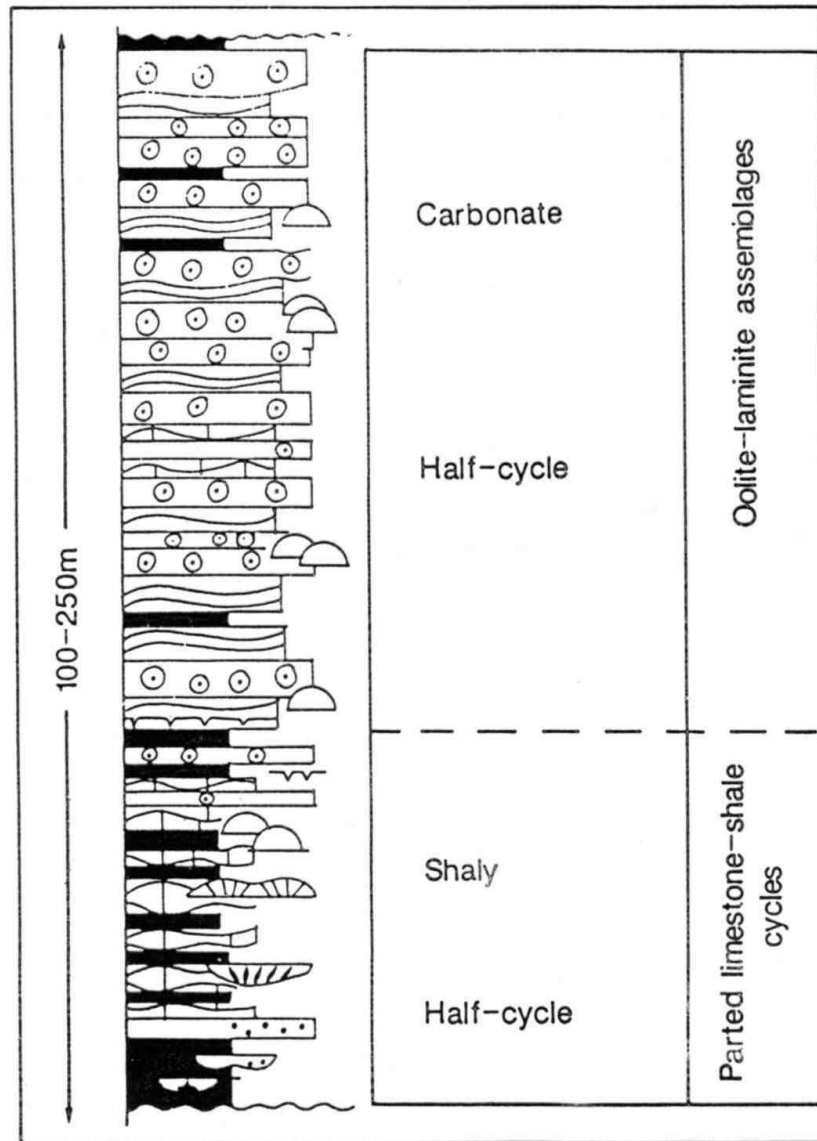
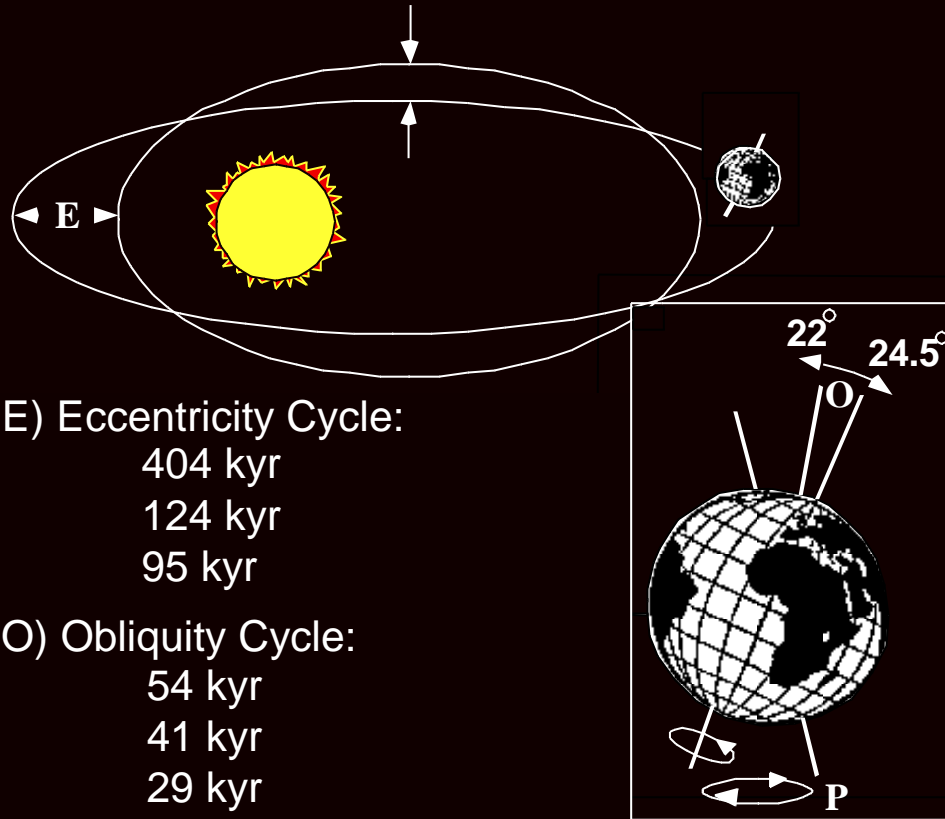


Fig. 2.29 Schematic Grand Cycle from the Cambrian of eastern North America consisting of many shale-limestone, shallowing-upward cycles in the lower part and oolite-stromatolite cycles in the upper part. After Chow & James (1987a).

Milankovitch Orbital Cyclicality



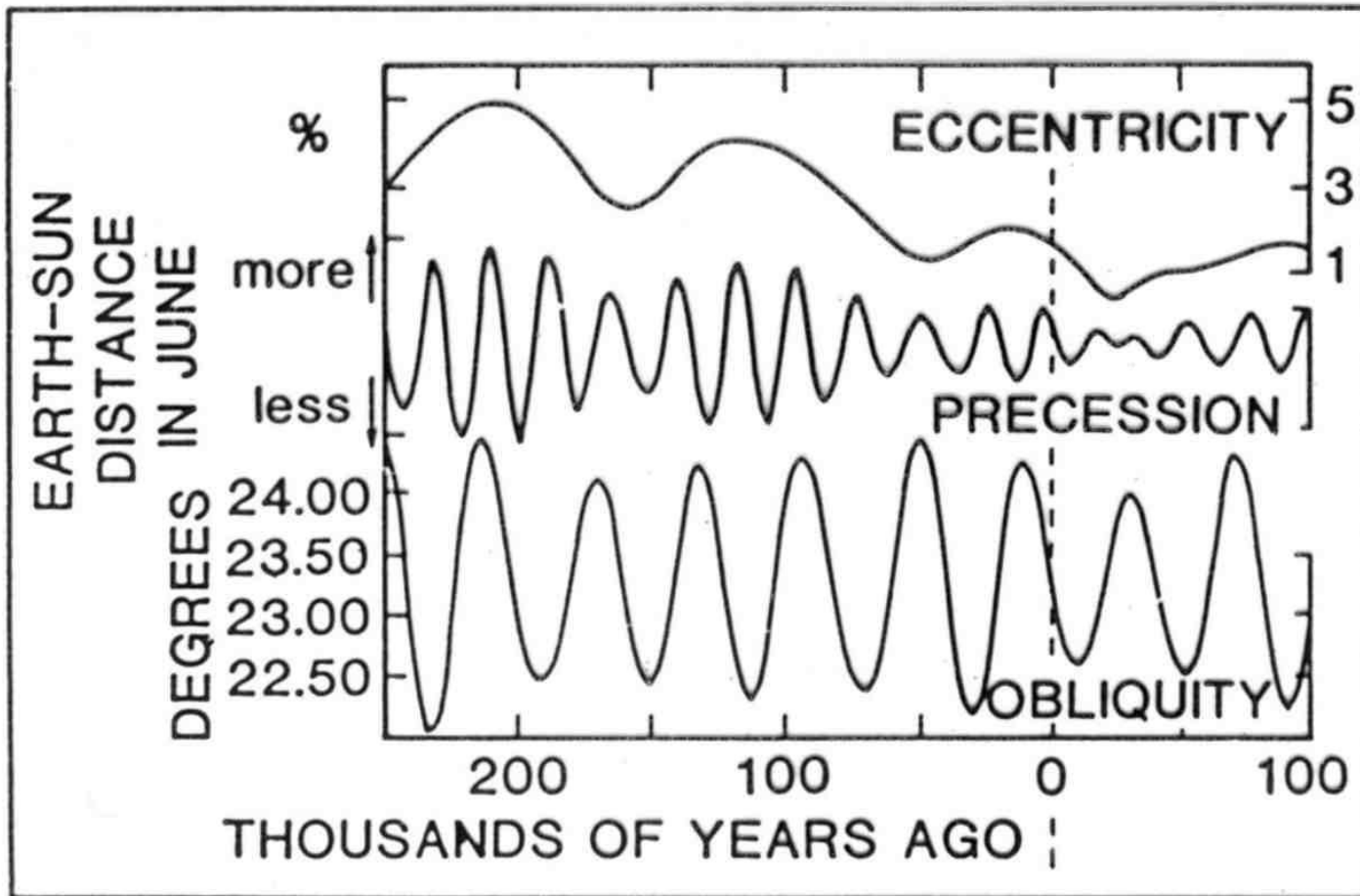
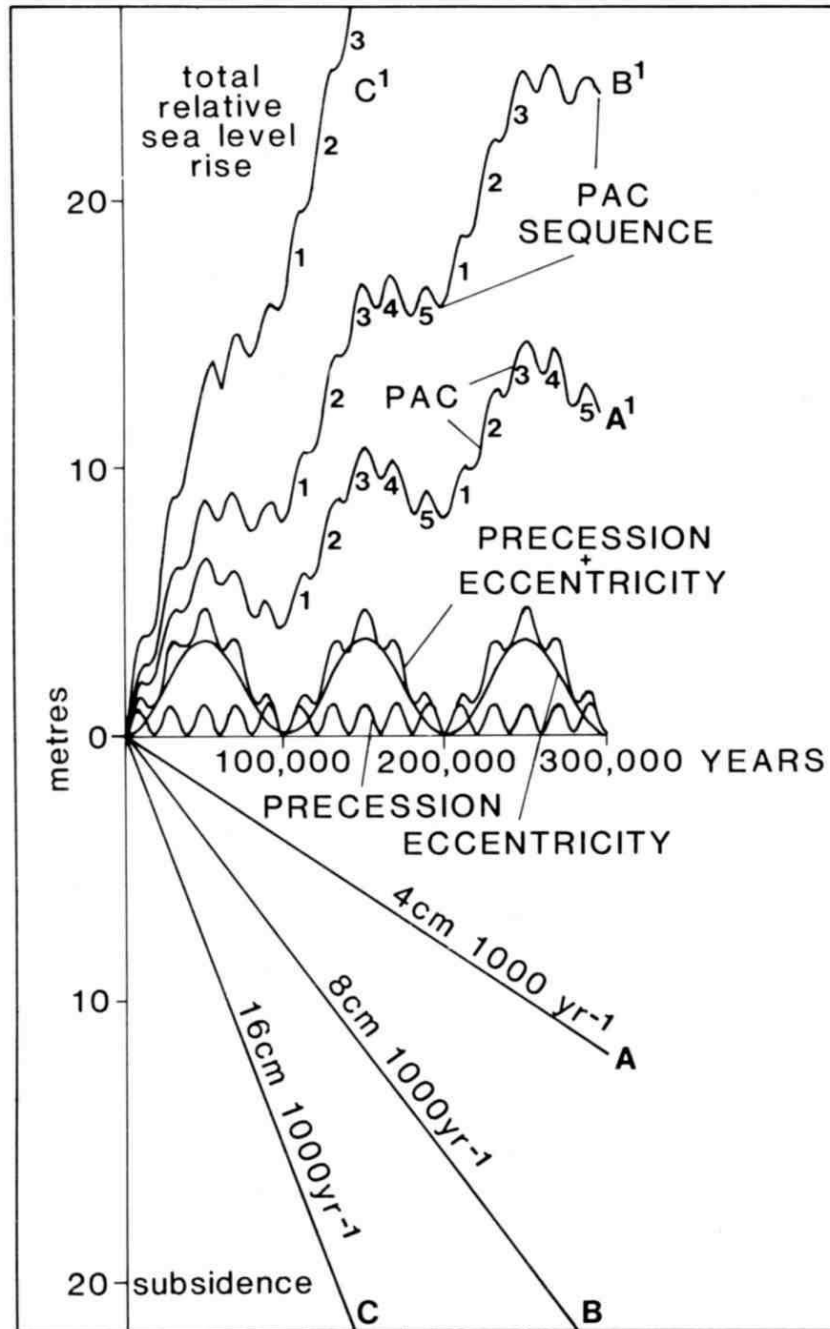


Fig. 2.30 *Milankovitch rhythms of the last 250 000 years, and into the future. After Imbrie & Imbrie (1980).*



čtení:

M.E.Tucker: Sedimentary petrology. 3rd ed. Blackwell, 2001(2003).

P.A.Scholle et al. (eds): Carbonate depositional environments. AAPG
Memoir 33, 1983.